Design of active sites in carbon materials for electrochemical potassium storage

GENG Chao[1], CHEN Ya-xin[1,*], SHI Li-luo[2], SUN Zong-fu[1], ZHANG Lei[3], XIAO An-yong[1], JIANG Jiang-min[1], ZHUANG Quan-chao[1], JU Zhi-cheng[1,*]

(1. *School of Materials Science and Physics*, *China University of Mining and Technology*, *Xuzhou* 221116, *China*;
2. *School of Materials and Chemical Engineering*, *Xuzhou University of Technology*, *Xuzhou* 221018, *China*;
3. *School of Materials Science and Engineering*, *Northeastern University*, *Shenyang* 110819, *China*)

Abstract: Carbon materials have attracted considerable attention as anodes for potassium ion batteries owing to their low-cost, nontoxicity, and controllable structures. The potassium storage behavior of carbon materials is highly associated with their active sites. In recent years, significant advances have been made in designing the active sites of carbon materials to meet the requirements of different potassium-based storage devices. Here, potassium storage mechanisms (intercalation and adsorption) for guiding the rational design of carbon materials are discussed. Based on these mechanisms, the review provides fundamental insight into the relationship between the structures and potassium storage performance of different carbon materials, including graphite, soft carbon, hard carbon, porous carbon, heteroatom-doped carbon, hybridized carbon and composited carbon. The structural design principles of carbon anode materials for potassium-ion full cell and potassium-ion capacitors are summarized based on the initial coulombic efficiency, capacity, potential plateau, rate performance, and cyclic stability. Finally, the problems and future research directions for the design of active sites in carbon materials for electrochemical potassium storage are considered.

Key words: Carbon materials; Active site; Potassium-ion battery; Anode materials

1 Introduction

The rapid consumption of traditional fossil fuel resources and serious global environmental pollution has caused many issues for the development of contemporary society[1,2]. Therefore, the development of clean energy is a good choice to alleviate fossil fuel dependence, especially the electrochemical energy storage (EES) system has received extensive attention[3–5]. In the EES system, lithium-ion battery (LIB) is the most mature one and has been widely used in electronic products, automotive and aerospace fields[1,6]. However, large-scale lithium-based energy storage equipment is restricted due to the scarce resources and their uneven distribution, and arduous recycling of lithium[7–9]. Thus, potassium-ion batteries (PIBs) with attractive/unique properties, such as low cost, abundant resources and relatively low reduction potential of potassium, have gained extensive attention in recent years[4,10,11]. At the same time, K^+ possesses the smallest Stokes' radius (0.36 nm) compared to Li^+ (0.48 nm) in propylene carbonate solvents, indicating that it has the highest ion mobility and ion conductivity[12,13]. The above advantages make potassium-based energy storage equipment an ideal candidate for green energy storage.

Carbon materials are considered to be the most promising anode materials for realizing K^+ storage owing to the obvious advantages of low cost, good electrical conductivity, controlled surface chemistry and structure[14–16]. The potassium storage active sites are highly correlated with the electrochemical potassium storage behavior and even performance[17]. Based on the different potassium storage sites, carbon materials have two typical potassium storage mechanisms, including intercalation and adsorption[1]. In general, the sloping region in the charge-discharge curve is determined by surface-driven K^+ storage, and the low-potential plateau region is driven by K^+ intercalation[14,18,19]. Graphite is a typical K^+ host by in-

Received date: 2022-03-21; **Revised date:** 2022-04-21

Corresponding author: CHEN Ya-xin, Ph.D, Lecturer. E-mail: chenyxcumt@163.com;
JU Zhi-cheng, Ph.D, Associated Professor. E-mail: juzc@cumt.edu.cn

Author introduction: GENG Chao, Master Student. E-mail: 17865813101@163.com

tercalation to form compound KC_8, which has a theoretical capacity of 279 mAh g^{-1} and an intercalation potential platform of about 0.3 V[20,21]. As a PIB anode material, graphite exhibits low discharge potential and high initial coulomb efficiency (ICE), which is beneficial for the construction of high energy density full-cells. However, during the charging and discharging process, the large size of K^+ (0.138 nm) produces volume expansion in graphite, resulting in cycle instability, capacity fading and poor rate performance[22,23]. Carbon structural engineering of graphitic materials can improve the K^+ storage capacity and cycling stability[24] by expanded interlayer spacing[25,26], heteroatom doping[27] and building composite structures[28,29].

Enhancing the K^+ adsorption capability at the active sites on the material surface by producing abundant carbon defects or large specific surface area (SSA) is an effective strategy to improve the potassium storage performance of carbon materials[30,31]. Abundant active sites on the carbon surface can increase the K^+ accumulation space and fast kinetics, resulting in high capacity and excellent rate performance of carbon anode materials[32,33]. Based on these significant advantages, much progress has been achieved in the design and development of various types of anode materials, including morphology adjustment (porous, nanosheets, nanofibers)[16,34–37], structural design (disordered structures, hybridized structures)[2,10,38], and heteroatom doping[39,40]. But, the low ICE, high-potential sloping curves, and low material density should be cautiously considered for practical applications[41]. It is found that the variation of active potassium storage sites leads to different potassium storage mechanisms, and further influences the potassium storage performance. Therefore, the intercalation and surface-driven potassium storage of different active sites should be fully considered in the design of carbon structures to optimize the performance. At the same time, it should also be focused on the assembly of full device corresponding to the appropriate mechanisms and electrodes.

In this review, a detailed summary of the relationship between active sites and potassium storage mechanism/performance of carbon materials has been discussed (Fig. 1). The influence of carbon structure evolution during potassium storage is introduced in detail in terms of graphite, soft carbon and hard carbon materials. Based on that, we review the design strategies, including porous structure, heteroatom doping, hybrid structure and composite structure for carbon materials aiming at boosting electrochemical performance. Finally, the potassium storage devices with different carbon electrode materials are summarized, and the challenges and prospects for further development of carbon anodes are put forward.

2 Potassium storage mechanism of active sites

Active sites of carbon materials are particularly important for K^+ storage in carbon materials. Potassium storage active sites mainly include graphitic layers, edges and defects, which can be divided into two mechanisms: intercalation/deintercalation and adsorption/desorption[22]. The K^+ intercalation/deintercalation mechanism occurs mainly in the carbon interlayers[42]. Due to the low discharge potential and high ICE of interlaminar materials, PIBs can possess high energy density in practical applications. However, the K^+ intercalation in carbon material will produce volume expansion, resulting in the loss of contact

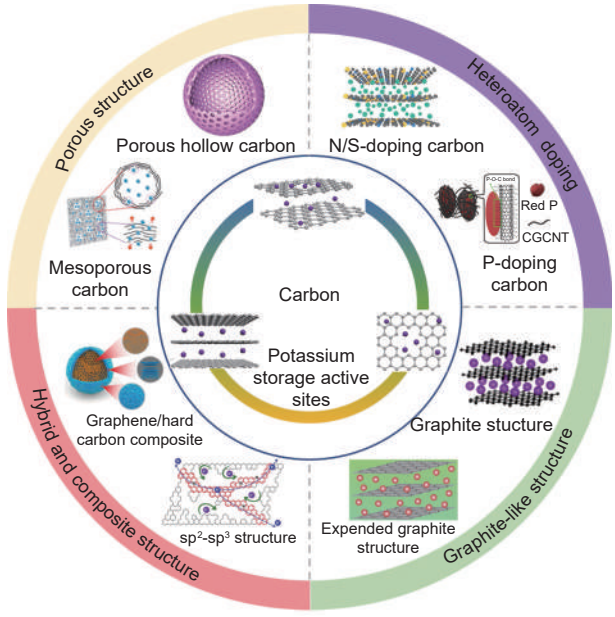

Fig. 1 Illustration of strategies to boost the electrochemical performance of carbon-based anodes and K^+ storage mechanism at carbon active sites.

between the active material and the collector, increasing interface resistance and deteriorating battery performance[9,43]. The adsorption/desorption of K^+ is mainly on the surface, pores and defects of carbon materials[44]. The storage of K^+ by adsorption is not limited by the electrode structure damage and the theoretical capacity of KC_8, showing high potassium storage capacity, superior rate performance and cyclability[18]. Therefore, the diffusion kinetics and adsorption capacity of K^+ can be boosted by increasing the specific surface area (SSA) and creating more defects. However, the large surface area and high defects will consume a large amount of the electrolyte to form a solid electrolyte film (SEI), resulting in high irreversible capacity and low ICE during the initial cycle. What's more, the active sites on the carbon surface break the integrality of the π conjunction of the carbon plane, which decreases the intrinsic conductivity[32]. As shown in Fig. 2, two typical potassium storage mechanisms are specifically compared in terms of their potassium storage performance.

Many efforts have been devoted to the development and design of carbon structures, which have revealed the potassium storage mechanisms in different carbon structures and achieved excellent electrochemical performance. The electrochemical performance of carbon materials, including capacity, potential platform, rate capability, ICE and cycle stability is shown in Table 1.

3　Effect of carbon structure evolution on the potassium storage behavior

An in-depth understanding of the potassium storage mechanism at different active sites is necessary for designing material structures for performance requirements. Rationally controlling the intercalation and adsorption behavior of the carbon structures to achieve a balance of material properties is essential yet challenging to the reasonable allocation of the two mechanisms. The carbon structure evolves with the heat treatment temperature (HTT), which significantly affects the potassium storage behaviors[67]. For graphite, the structure stability and the kinetics during cycling can be boosted by adjusting the graphite interlayer distances, further enhancing the cyclic stability and the rate performance. For both hard and soft carbons, regulating the carbon structure by controlling the pyrolysis temperature is an effective way to improve the K^+ storage performance (Fig. 3). Generally, K^+ storage behavior exhibits a tendency from adsorption on carbon surfaces or edges at low HTT to intercalation in the carbon layers at high HTT. Correspondingly, the electrochemical properties of potassium storage also change with HTT, such as the capacity, rate performance, cycling stability, ICE and potential plateau of the carbon material.

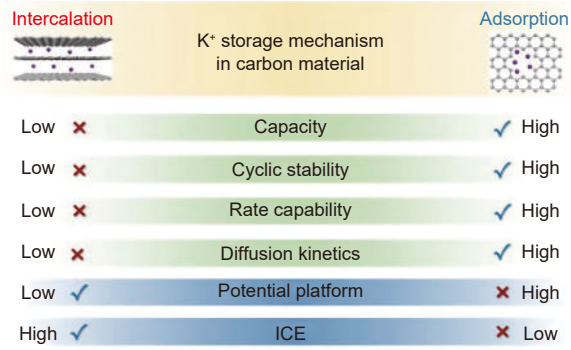

Fig. 2　Schematic illustration of the intercalation-controlled and surface-driven capacitive K^+ storage with their respective strengths and weaknesses.

3.1　Graphite

Graphite is composed of stacked graphene layers, which is a typical representative of the intercalation reaction in anode materials. K^+ can intercalate into the interlayers of graphite to form a series of intercalated compounds with the theoretical capacity of 279 mAh g^{-1}[68]. Moreover, the formation sequence of these intercalated compounds is closely related to the process of potassium intercalation. Ji et al.[45] investigated the K^+ intercalation/deintercalation mechanism in the interlayers of graphite by *ex-situ* XRD, revealing the formation stage of KC_{36} - KC_{24} - KC_8 (Fig. 4a, 4b). On this basis, Fan et al.[69] discovered firstly the KC_{48} peak at 23°/29° by *in-situ* XRD, which clarifies the types of KC_x intercalation compounds in the charge/discharge process (Fig. 4c, 4d). In addition, four peaks of 0.37 V, 0.34 V, 0.24 V and 0.16 V were identified, corresponding to the transition stage of KC_{48}, KC_{36}, KC_{24} and KC_8 (Fig. 4e).

Graphite possesses a low potential plateau during charging/discharging. However, the large K^+ has

Table 1 A comparison of the K^+ storage performance for different carbon materials.

Materials	Capacity ($mAh\ g^{-1}$)	Potential (V)	ICE (%)	Rate capability ($mAh\ g^{-1}$)	Capacity retention	Mass loading ($mg\ cm^{-2}$)	Ref.
Graphite							
Graphite	273 at 0.028 A g^{-1}	~ 0.2	57.4	80 at 0.28 A g^{-1}	50.8% after 50 cycles	~ 2	[45]
Expanded graphite	267 at 0.05 A g^{-1}	~ 0.3	81.6	175 at 0.2 A g^{-1}	99% after 500 cycles	~ 2	[26]
N-doped graphitic carbon	266 at 0.05 A g^{-1}	~ 0.3	48.7	228.9 at 2 A g^{-1}	188.9 after 2200 cycles	1-1.1	[46]
Polynanocr-ystalline graphite	224 at 0.02 A g^{-1}	~ 0.2	54.1	99 at 0.2 A g^{-1}	50% after 240 cycles	~ 2	[47]
Graphite	260 at 0.028 A g^{-1}	~ 0.3	81.5	250 at 1.4 A g^{-1}	99.9% after 300 cycles	~ 0.7	[48]
Soft carbon							
Soft carbon	264 at 0.028 A g^{-1}	~ 0.5	56.4	140 at 1.4 A g^{-1}	81.4% after 50 cycles	~ 2	[45]
N-doped carbon nanofibers	248 at 0.025 A g^{-1}	~ 0.65	49	101 at 20 A g^{-1}	\	~ 1.5	[49]
N-doped soft carbon	303 at 0.05 A g^{-1}	~ 0.5	30.9	141 at 5 A g^{-1}	85.5% after 500 cycles	~ 1	[50]
N/S-doped soft carbon	359 at 0.1 A g^{-1}	~ 0.5	50	115 at 5 A g^{-1}	79.5% after 200 cycles	1-1.2	[51]
Pitch-derived soft carbon (1200 °C)	296 at 0.028 A g^{-1}	~ 0.2	65	115.2 at 1.4 A g^{-1}	93.2% after 50 cycles	\	[52]
Pitch-derived soft carbon (1400 °C)	194 at 0.025 A g^{-1}	~ 0.27	70	110 at 0.5 A g^{-1}	75% after 100 cycles	~ 2	[53]
Pitch-derived soft carbon (1500 °C)	240 at 0.028 A g^{-1}	~ 0.24	\	80 at 1.4 A g^{-1}	67.9% after 500 cycles	~ 2	[19]
Hard carbon							
Rhodanine-derived hard carbon	425 at 0.05 A g^{-1}	\	\	237.4 at 1 A g^{-1}	90.4% after 10^{th} to 400^{th} cycles	~ 0.7	[10]
Biomass-derived hard carbon	442.4 at 0.03 A g^{-1}	~ 0.6	\	175 at 2 A g^{-1}	\	~ 0.17	[54]
quantum dots in hard carbon	325 at 0.1 A g^{-1}	\	39	110 at 1 A g^{-1}	75% after 150 cycles	~ 0.3	[38]
N/S-doped hard carbon	250 at 0.1 A g^{-1}	~ 0.5	35.2	174 at 3 A g^{-1}	66% after 1200 cycles	\	[55]
N/O-doped hard carbon	230 at 0.05 A g^{-1}	\	45.4	118 at 3 A g^{-1}	72% after 1100 cycles	~ 0.9	[39]
N/P-doped hard carbon	312 at 0.05 A g^{-1}	\	44	179 at 5 A g^{-1}	80% after 500 cycles	\	[56]
Porous carbon							
Porous hard carbon	237.6 at 0.1 A g^{-1}	~ 0.8	44.4	81.6 at 2 A g^{-1}	\	1.2-1.6	[57]
Porous hard carbon	259 at 0.05 A g^{-1}	~ 0.5	44.6	214 at 2 A g^{-1}	84% after 5000 cycles	1.1-1.3	[58]
Mesoporous carbon	460 at 0.05 A g^{-1}	\	\	110 at 4 A g^{-1}	71.3% after 2000 cycles	0.8-1.2	[16]
Nanocapsules carbon	293 at 0.05 A g^{-1}	~ 0.5	30.9	151 at 5 A g^{-1}	85.5% after 500 cycles	~ 1.	[50]
N/S co-doped nanocapsules carbon	408 at 0.05 A g^{-1}	\	33	149 at 5 A g^{-1}	81% after 10^{th} to 2000^{th} cycles	~ 1.2	[36]
N/P co-doped porous carbon	301 at 0.025 A g^{-1}	~ 0.5	60.04	126 at 10 A g^{-1}	81.8% after 400 cycles	1-1.4	[59]
Hierarchical porous carbon	211.5 at 0.05 A g^{-1}	\	24.1	76.7 at 10 A g^{-1}	53% after 100 cycles	0.8-1	[60]
Heteroatom-doping carbon							
N-doped carbon	248 at 0.025 A g^{-1}	~ 0.65	49	101 at 20 A g^{-1}	\	~ 1.5	[49]
S-doped carbon	310 at 0.05 A g^{-1}	~ 0.75	42	182.7 at 2 A g^{-1}	68% after 2000 cycles	~ 2.4	[61]
P-doped carbon	323.5 at 0.05 A g^{-1}	~ 0.5	50.3	90 at 0.5 A g^{-1}	53.7% after 500 cycles	\	[62]
P-doped carbon	402.6 at 0.1 A g^{-1}	~ 0.75	\	258 at 1 A g^{-1}	\	\	[40]
N/O co-doped carbon	365 at 0.025 A g^{-1}	\	38	118 at 3 A g^{-1}	69.5% after 1100 cycles	~ 0.9	[39]
N/S co-doped carbon	359 at 0.1 A g^{-1}	\	50	115 at 5 A g^{-1}	92% after 1000 cycles	1-1.2	[51]
Hybrid and composite carbon							
sp^2-sp^3 carbon	425 at 0.05 A g^{-1}	\	\	237.4 at 1 A g^{-1}	90.4% after 10^{th} to 400^{th} cycles	~ 0.7	[10]
sp-sp^2 carbon	505 at 0.05 A g^{-1}	\	\	150 at 5 A g^{-1}	90% after 2000 cycles	~ 0.8	[102]
Hard-soft carbon	376.8 at 0.025 A g^{-1}	~ 0.68	71.0	101.2 at 4 A g^{-1}	\	~ 1.2	[63]
Graphite-soft carbon	280 at 0.028 A g^{-1}	~ 0.8	67.3	\	\	2-2.5	[28]
Graphite-hard carbon	253 at 0.05 A g^{-1}	~ 0.18	61.8	215.7 at 0.2 A g^{-1}	97.5% after 1000 cycles	\	[29]
Graphene-hard carbon	297.89 at 0.1 A g^{-1}	~ 0.25	\	220 at 1 A g^{-1}	99.4% after 3200 cycles	~ 1.2	[66]

sluggish kinetics and produces volume expansion of *ca.* 61% when it is intercalated into the interlayers of graphite, which leads to serious capacity fading and low-rate performance[45]. To enhance the stability of graphite structures during intercalation/deintercalation of K^+, a highly graphitic carbon nanocage (CNC) was designed by Cao and co-workers[64]. Benefiting from the hollow cage structure to buffer the volume change and reduce the K^+ diffusion length, CNC exhibited superior depotassiation capacity of 175 mAh g^{-1} at 35 C (1 C = 279 mA g^{-1}). Feng et al.[26] reported that commercial graphite (CG) had a discharge capacity of 202 mAh g^{-1} and 60% ICE (Fig. 4f). The reversible capacity decreased from 169 to 61 mAh g^{-1}

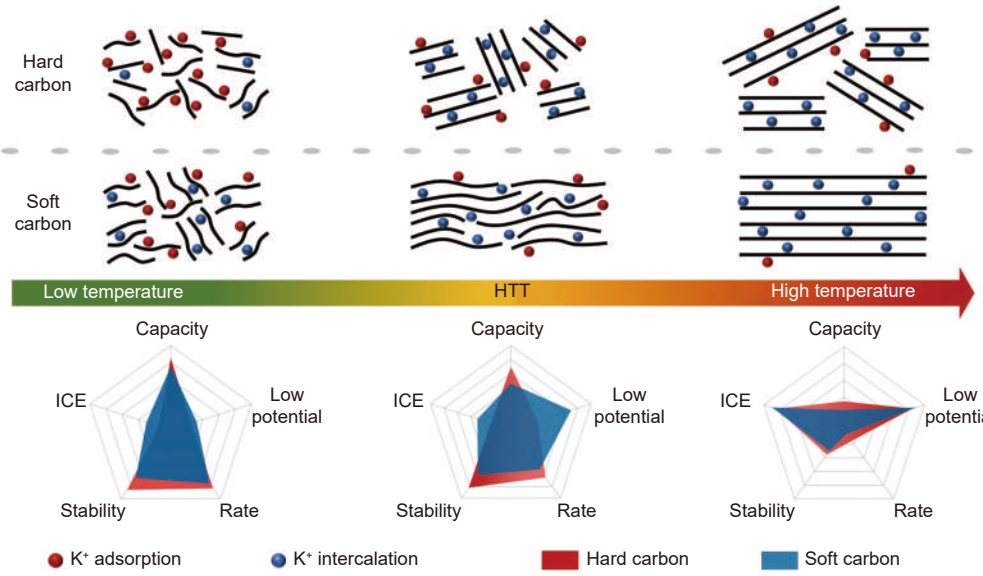

Fig. 3　Effects of hard/soft carbon structure evolution on K^+ storage behavior and properties.

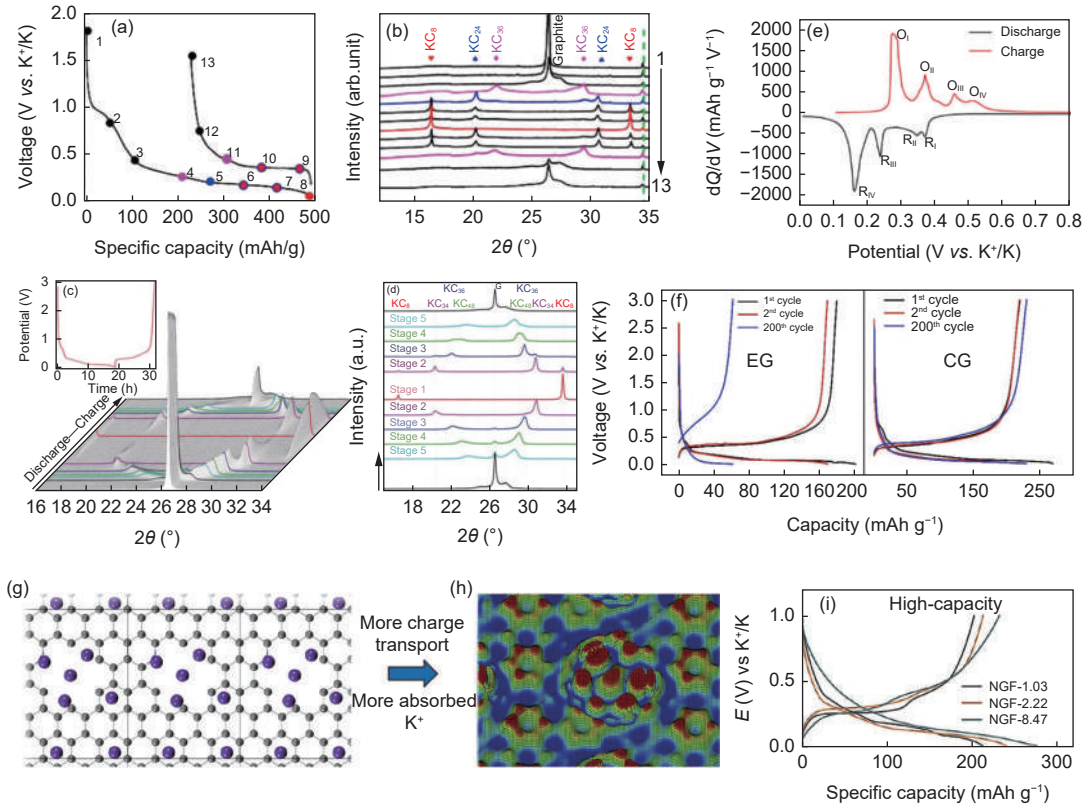

Fig. 4　(a) The initial discharge/charge profile of a graphite electrode at C/10 (1 C = 279 mA g^{-1}) and (b) XRD patterns of electrodes corresponding to the marked stage compounds of charge in panel (a)[45]. (c) Waterfall representation XRD patterns at the first cycle and (d) the selected XRD patterns during the initial discharge/charge with different stages. (e) The dQ/dV profiles[69]and (f) galvanostatic charge/discharge voltage profiles at 50 mA g^{-1} of CG and EG[26]. (g) The structure of high-density K adsorbed around pores in graphene. (h) Electron charge density distribution differences and (i) the galvanostatic charge/discharge profiles of the NGF electrode[70](Reproduced with permission).

after 200 cycles. Regulating the structure of graphite material alleviates the structural instability caused by K^+ intercalation. As shown in Fig. 2f, the expanded graphite (EG) with wide interlayer distances possessed a discharge capacity of 267 mAh g^{-1} with a CE of 80.83% during the initial cycle. After 200 cycles, the reversible capacity remained at 228 mAh g^{-1} with a capacity retention rate of 105.07%. Tai et al.[65] ex-

panded the interlayer spacing from 0.334 to 0.358 nm by activating the graphite with KOH, resulting in a graphite electrode with a high reversible capacity of 100 mAh g^{-1} in 100 cycles at 200 mA g^{-1}. Moreover, Shen et al.[70] concluded that N-doping in graphite foam facilitated K^+ storage by theoretical calculations (Fig. 4g). Benefiting from more K^+ adsorption and faster charge transfer (Fig. 4h), capacity retention of 247 mAh g^{-1} after 200 cycles was accomplished (Fig. 4i). The above methods can improve the diffusion kinetics of K^+ between graphite layers by optimizing the graphite structure, which leads to the graphite anode materials with superior electrochemical potassium storage performance.

3.2 Soft carbon

Soft carbon with a turbostratic structure that is convertible into graphite at high temperatures and is beneficial to K^+ storage due to the large interlayer spacing and multiple carbon edges[52,71]. The turbostratic carbon structure possesses a good arrangement of carbon layers, resulting in superior electrical conductivity[18]. Moreover, soft carbon can be converted into graphite after annealing at HTT higher than 2 500 °C, which is of significant value for studying the storage mechanism and electrochemical properties of K^+ through structural evolution. Zhang et al[53]. investigated the correlation between the order degree of soft carbon and the corresponding K^+ storage as shown in Fig. 5a. Two main K^+ storage mechanisms were identified in soft carbon, adsorption at carbon edge/defect sites and intercalation into the interlayers. On this basis, Lu et al.[19] determined that the capacity in the voltage range of 0.45-1.1 V originates from the K^+ adsorption at the edge/defect sites, while capacity below 0.45 V is attributed to the insertion of K^+ (Fig. 5b). In addition, the proportion of sloping regions gradually decreases with the increase of HTT, and plateau regions appear at 0.23 V at 1 500 °C. When HTT is further increased to 2 800 °C, the sloping region disappears and the charging/discharging potential platform is below 0.23 V (Fig. 5c). Fig. 5d shows the intercalation mechanism of K^+ in soft carbon[52]. With the beginning of the discharge process, the (002) peak disappears rapidly and the graphitization characteristics decrease due to K^+ intercalation. The preparation of soft carbon from pitch by carbonization at 1 200 °C (SC-1200) shows shoulder peaks with no impurity phase and the emergence of tiny KC_8 peaks at around 0.14 V. Furthermore, the electrochemical behavior of three typical samples (SC-1200, hard carbon and graphite) is compared, among which SC-1200 displays advantages as PIB anodes with a high reversible capacity of 296 mAh g^{-1} and 93.2% of the initial capacity remained at 0.1 C (1 C = 279 mA g^{-1}) after 50 cycles (Fig. 5e). Ou et al.[72] found that the potential plateau is closely correlated to non-uniformity in the interlayer distance and defect density in soft carbon (Fig. 5f). The widely distributed scattering peaks in the wide-angle X-ray scattering (WAXS) pattern (Fig. 5g) indicate that the non-uniformity of the interlayer distance is closely associated with the defects. With the increase of HTT, the non-uniformity in the interlayer distance decreases and the potential platform is enhanced. Moreover, as shown in Fig. 5h, a soft carbon with a higher defect density possesses a higher discharge potential platform as demonstrated by DFT calculation.

Regulating the carbon structure by adjusting the HTT is an effective way to reveal the intercalation/adsorption hybrid mechanisms of K^+. The K^+ storage mechanisms of the carbon nanofibers (CNFs) were explored from 650, 1 250 to 2 800 °C using polyacrylonitrile as the precursor (Fig. 6a)[67]. As shown in Fig. 6b, partially ordered carbon displays intercalation and adsorption hybrid behavior of K^+ at 1 250 °C in contrast to the single potassium storage mechanism of disordered carbon treated at 600 °C and the intercalation mechansim of graphitic carbon treated at 2 800 °C. The *in-situ* Raman (Fig. 6c) and *in-situ* XRD (Fig. 6d) spectra show that the peak of CNF-1250 is well maintained without significant positional shifts during discharging/charging process. In contrast, CNF-2800 displays a clear peak of the KC_8 compound (Fig. 6e). The above results indicate that the K^+ storage mechanism in CNF-650 is dominated by surface adsorption, and that in CNF-2800 is driven by interlayer intercalation. Based on this hybrid potassium storage mechanism, the authors further investigated the sensitivity of the anode material to the test temper-

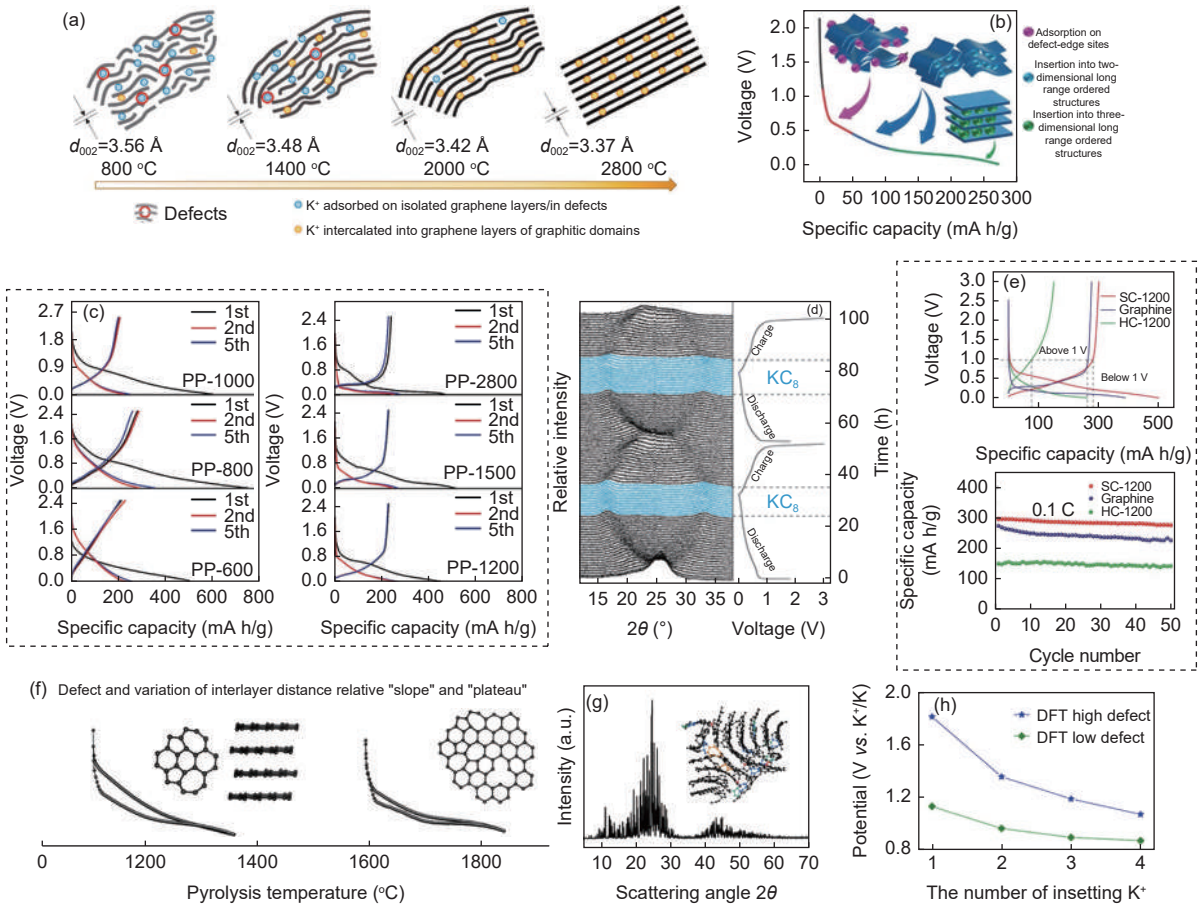

Fig. 5　(a) Correlation between the microstructure of soft carbon and HTT[53]. (b) The potassium storage mechanism of soft carbon at different stages during discharge. (c) Discharge/charge curves of soft carbon at different HTTs for cycles 1, 2 and 5[19]. (d) The *in-situ* XRD spectra of SC-1200. (e) The discharge/charge profiles in the 1st cycle and cyclability test at 0.1 C of SC-1200, graphite, and HC-1200[52]. (f) Schematic diagram of the major determinants affecting potential profiles of potassium storage. (g) Typical structure fragment and the calculated WAXS pattern based on RMC modeling. (h) Effect of the defect concentration on potential revealed by DFT calculation[72](Reproduced with permission).

ature. When the temperature drops to 0 °C, the capacity retention of CNF-1250 is 79.7%, while that of CNF-650 and CNF-2800 is 75.2% and 60.8% (Fig. 6f), respectively, indicating that the hybrid mechanism is more insusceptible to the working temperature.

3.3　Hard carbon

The carbon microcrystals within the hard carbon possess a low accumulation of carbon lamella along the c-axis (L_c) and exhibit an overall random orientation arrangement[42]. As hard carbon materials are difficult to graphitize even above 2 500 °C, many nanographitic domains such as edges and defects exist in the hard carbon[14]. Thus, the potassium storage mechanism in hard carbon materials is complex. In this regard, many efforts have been contributed to exploring the relationship between the microstructures of hard carbon materials and potassium storage behaviors. Komaba et al.[73] directly observed the temperature-dependent microstructure of hard carbon and the corresponding selected area electron diffraction (SAED) using TEM (Fig. 7a, 7b). Compared with the HC700 (hard carbon prepared at 700 °C) sample, the HC2000 (hard carbon prepared at 2 000 °C) sample possesses advanced structural ordering and a relatively clearer diffraction ring. As shown in Fig. 7d, 7e, d_{002} decreases from 0.402 to 0.364 nm and L_c increases from *ca.* 0.7 to 1.3 nm in the HTT range of 700-2 000 °C. Simultaneously, the results reveal that the microstructure, morphology and elemental parameters of a hard carbon are strongly dependent on the HTT (Fig. 7c). Wang's work illustrated the relationship between the structure and potassium storage performance of hard carbon materials at different HTTs[74]. As the HTT

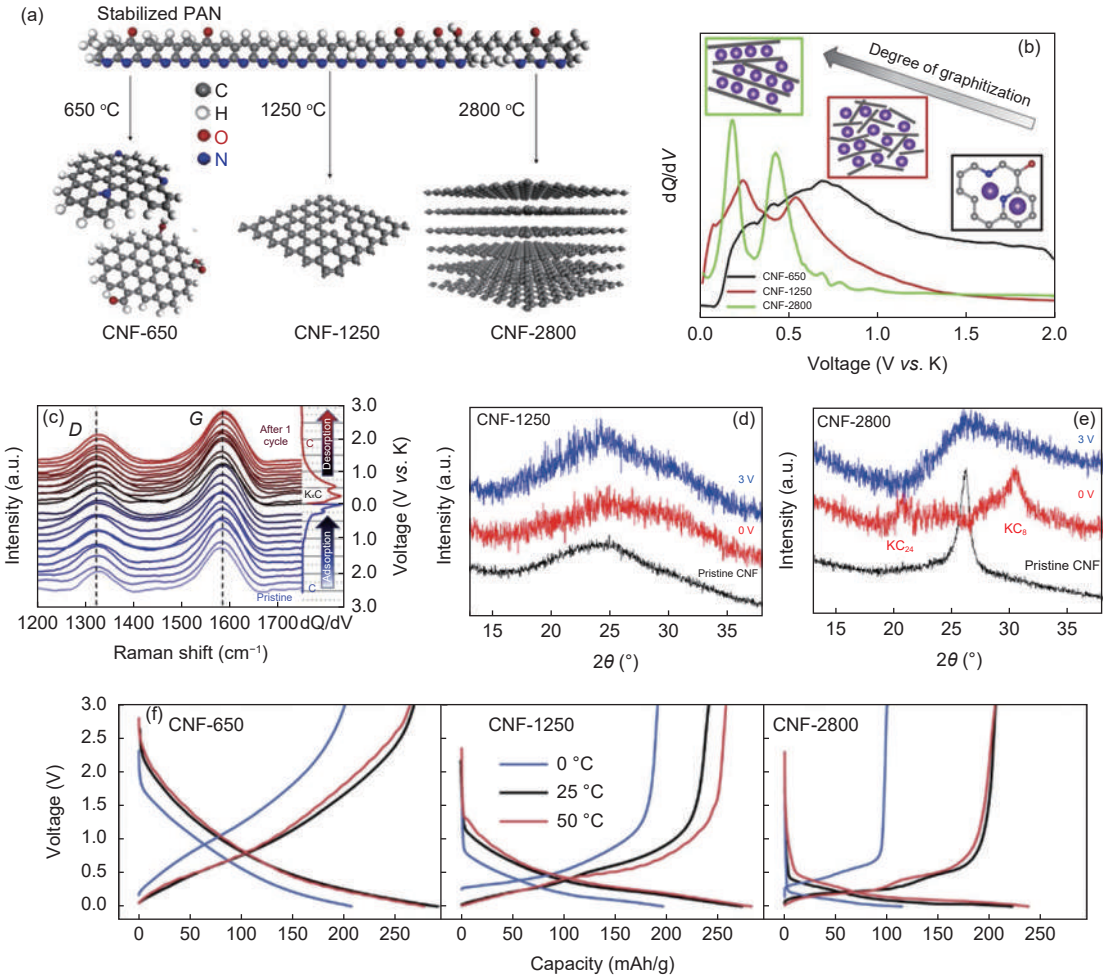

Fig. 6 (a) Correlation between the microstructure of CNFs and the annealing temperature. (b) The dQ/dV curves of CNF films after oxidation, the inset illustrates the main K^+ storage mechanism in three different regions. (c) Selective *in-situ* Raman spectra of CNF-1250 with corresponding dQ/dV plot. The *in-situ* XRD pattern recorded on the first discharge/charge for (d) CNF-1250 and (e) CNF-2800. (f) Discharge/charge curves of CNFs at different working temperatures[67](Reproduced with permission).

rises from 1 000 to 1 600 °C, the plateau region capacity (II-region) increases from 92 to 165 mAh g^{-1} (Fig. 7f). Meanwhile, the slope region capacity (I-region) decreases from 164 to 86 mAh g^{-1}. Correspondingly, the oxidation peak varies from 0.32 to 0.27 V, and reduction peak varies from 0.20 to 0.14 V with increasing HTT (Fig. 7g). Thus, the dominant potassium storage mechanism of hard carbon gradually varies from a surface-driven to an intercalation-controlled one as HTT rises, which is ascribed to the production of micro-graphite structures. It's worth noting that the hard carbon at 1 200 °C (SP-HC 1200) possesses a capacity of 284 mAh g^{-1}, which exceeds the theoretical capacity of graphite (279 mAh g^{-1}). This is because K^+ not only intercalates/deintercalates in microcrystalline graphite, but also adsorbs/desorbs on its surface and edges. As shown in Fig. 7h, the adsorption-dominated slope region (I-region) delivers additional potassium storage capacity, leading to superior rate capacity and excellent cycling performance of hard carbon. Similar results were also obtained by Kim and co-workers[75], K half-cell delivered the obvious sloping region (above 0.25 V) and quasi-plateau region (0.25 V). From 1 000 to 1 500 °C, the slope capacity decreases and the plateau capacity increases for hard carbons (Fig. 7i). Moreover, Wen et al.[38] reported a carbon quantum dots@hard carbon (CQDHC) composite electrode material for PIBs (Fig. 7j). It is found that randomly distributed carbon quantum dots (CQDs) can boost the disorder extent, enhancing the capacitive storage process driven by adsorption on the hard carbon surface.

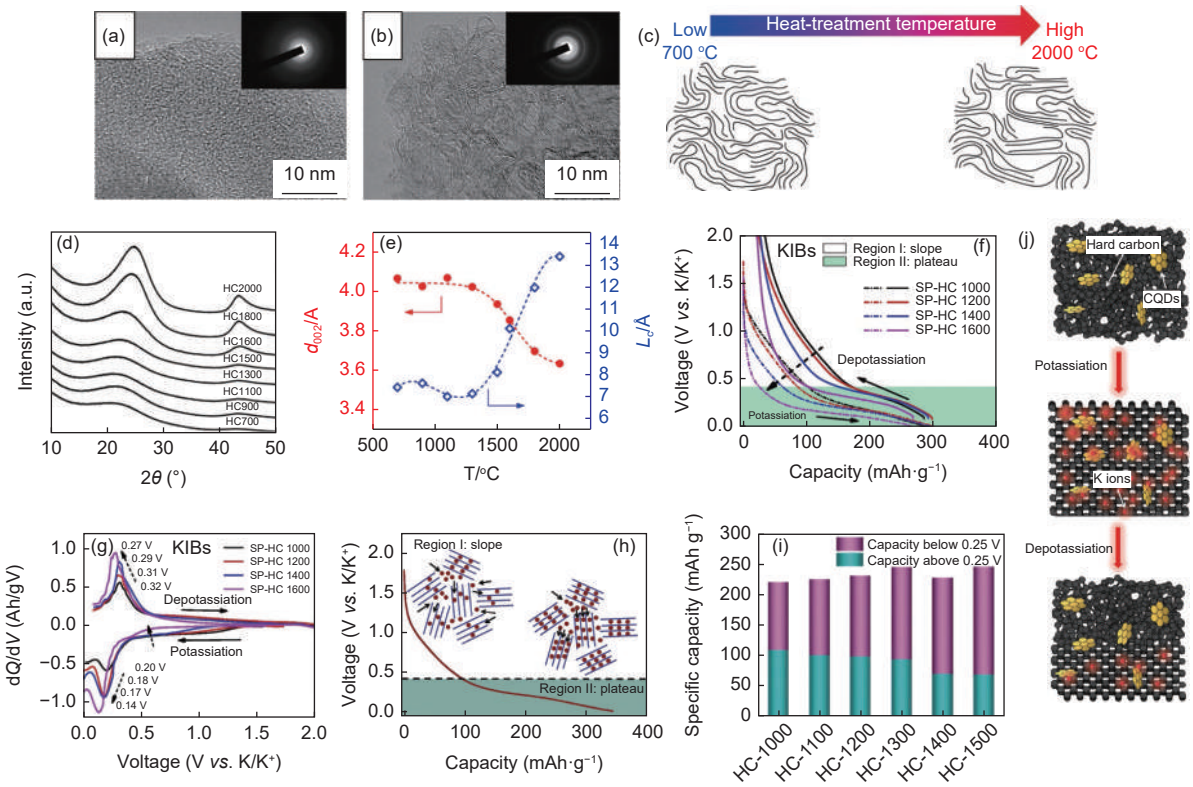

Fig. 7　TEM images and SAED patterns of hard carbon samples: (a) HC700 and (b) HC2000. (c) Schematic illustration of microstructures of the hard carbon samples prepared at 700 and 2000 °C. (d) Powder XRD patterns of carbon samples prepared at different HTTs. (e) Interlayer distances of carbon layers[73]. (f) The charge-discharge curves of SP-HCs. (g) The dQ/dV curves of SP-HCs. (h) The K^+ storage mechanism in hard carbon[74]. (i) the capacities of sloping-voltage and plateau-voltage regions in relation to HTT[75]. (j) Schematic diagram of K^+ storage mechanism in CQDHC[38](Reproduced with permission).

Anode materials with K^+ adsorption behavior generally possess a larger SSA and higher defects than intercalation/deintercalation ones. High SSA and defect-rich materials have higher capacity yet inevitably lower ICE[76]. Balancing the capacity and ICE is the key to overcoming this issue. Wang et al.[77] prepared carbon spheres with a nano-size and porous structure (SPCS) by the sol-gel method. SPCS displayed a higher SSA (398.85 $m^2\ g^{-1}$) compared to carbon spheres (CS, 76.02 $m^2\ g^{-1}$). However, SPCS with a high SSA delivers a higher ICE (68.2%) and capacity (232.6 mAh g^{-1}) than CS with a lower ICE (60.3%) and capacity (121.5 mAh g^{-1}). Mai et al.[2] developed a hard carbon with a high ICE by constructing interconnected mesoporous carbon (meso-C) nanowires. Compared with the SSA of micro-C (706.6 $m^2\ g^{-1}$), the SSA of meso-C (22.4 $m^2\ g^{-1}$) is reduced by *ca.* 32 times, which exhibited a high ICE of 76.7% and an excellent capacity of 231 mAh g^{-1} simultaneously. The above works demonstrate that the improvement of both ICE and capacity can be achieved through the structural design of hard carbon materials.

4　Structure design strategies of carbon materials

Based on the understanding of the potassium storage mechanism of different active sites, the rational design of a carbon anode material can effectively improve its electrochemical performance[78]. This paper specifically discusses the design strategies of several carbon structures, including porous structure, heteroatom-doping, hybrid structure and composite structure.

4.1　Porous structure

Introducing pores into the carbon materials is an effective strategy to enhance the electrochemical performance of carbon anodes. The introduction of pores will create defects in the carbon materials, which can induce the local charge density rearrangement of the carbon network to enhance the potassium storage capability[79,80]. Generally, the carbon materials can be de-

signed to obtain a rich pore structure to meet the potassium storage requirements[81]. Furthermore, many efforts have been contributed to the relationship between porous structures and K^+ storage behavior as well as electrochemical properties.

To reveal the K^+ storage mechanism in porous hard carbons (HCs), Li et al.[57] developed HCs with controlled micro/mesoporous structures by a template-assisted spray pyrolysis method (Fig. 8a). TEM images showed that the author successfully obtained three products, which were spherical carbon (HC-A, Fig. 8b), bowl-like carbon shell (HC-B, Fig. 8c) and flake-like composites (HC-C, Fig. 8d). Among them, HC-B possessed the largest pore volume (0.58 $cm^3\ g^{-1}$) and SSA (955.1 $m^2\ g^{-1}$) owing to the unique bowl-like structure, which contributed to the improved K^+ storage performance. Fig. 8g exhibits that the initial reversible capacities of HC-A, HC-B and HC-C are 78.6, 237.6 and 285.2 mAh g^{-1}, with corresponding ICE of 27.7%, 44.4% and 47.2%, respectively. It is concluded that ICE strongly depends on the mesopore volume (Fig. 8f). There is no evident correlation between ICE and SSA, suggesting that the effective potassium storage active sites are on mesopore wall. What's more, the authors provide insight into the K^+ storage mechanism by *in-situ* Raman characterization (Fig. 8h). HC-B manifests two distinct regions at about 0.8 V on the I_D/I_G ratio curve. They correspond to two different K^+ storage mechanisms: surface-driven capacitive storage at high potentials and intercalation storage mechanism at low potentials. The capacitive contribution dominates throughout the cycle in HC-B as revealed by quantifying the capacity of the two different storage mechanisms (Fig. 8i). Meanwhile, the schematic diagram of the K^+ storage mechanisms in porous HCs are presented, including absorption on the active sites, trapping at micropores and intercalation between the graphene layers (Fig. 8j). Recently, Yuan et al.[58] also unraveled the correlation between micro/mesopores and K^+ migration behavior in HCs. It was confirmed that the micropores provided additional active sites for K^+ adsorption. A large number of mesopores could also provide pathways for K^+ intercalating, thereby improving ICE and intercalation capacity. Moreover, Zhang et al.[16] concluded that the introduction of mesopores can create a large number of defects, such as graphene edges and voids, which are active sites for K^+ storage.

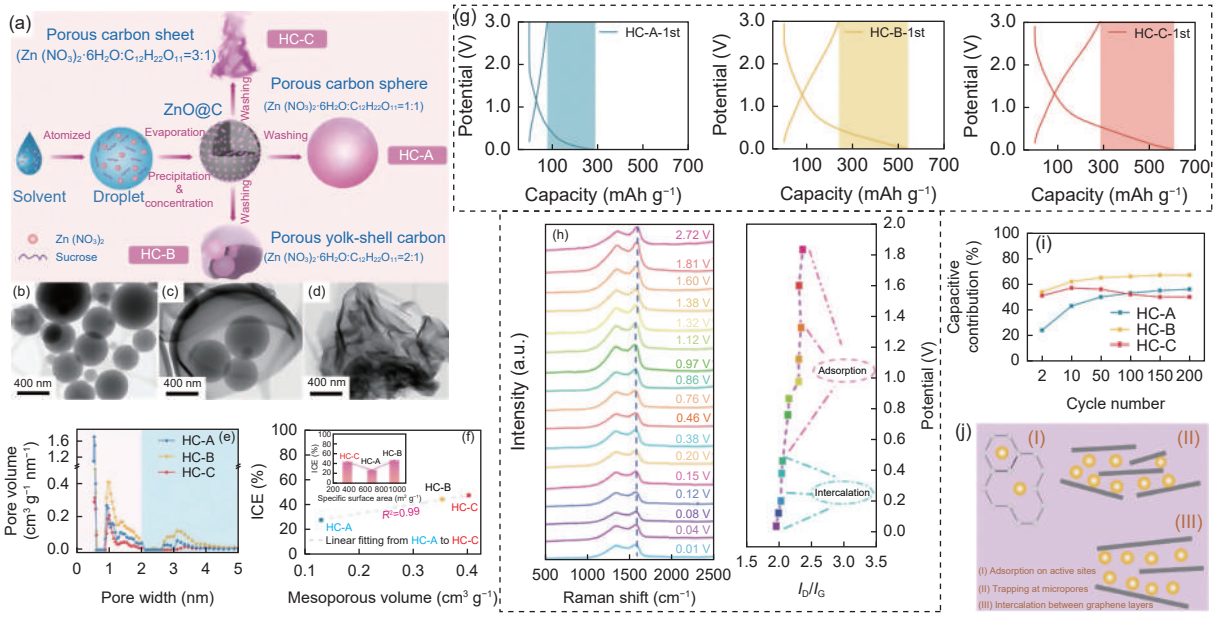

Fig. 8 (a) Schematic diagram of the synthesis procedure for the porous carbons *by* spray pyrolysis. TEM images of (b) HC-A, (c) HC-B and (d) HC-C. (e) Pore size distribution curves, (f) relationship between mesopore volume and ICE and (g) first charge/discharge curves of HC-A, HC-B and HC-C electrode at 0.1 A g^{-1}. (h) *In-situ* Raman spectra of the HC-B electrode, and the corresponding variation of I_D/I_G ratio. (i) Capacitive contribution of different HCs during cycling process. (j) Scheme illustration of K^+ storage mechanisms in HCs[57](Reproduced with permission).

The preparation methods of porous carbons are simple and diverse, which have promising applications in PIB anode materials[82]. The template method is a common method to obtain porous carbons due to its low cost, simple method and accurate adjustment[83,84]. As shown in Fig. 9a, Qiu group[36] synthesized 3D N/S co-doped carbon nanocapsules (NSCN) by ZnO templating. TEM image (Fig. 9b) confirms that NSCN possesses carbon nanocapsules with a 3D morphology. Moreover, the nanocapsule size can be varied by the sizes of the ZnO template. Similarly, Liu et al.[50] designed a carbon negative electrode of a nanocapsule-like shape (NSCN) by MgO templating, resulting in excellent rate performance (151 mAh g^{-1} at 5 A g^{-1}). In addition, metal organic frameworks (MOFs) have become effective precursors for porous carbons. For example, Liu et al.[82] developed N-rich hollow carbon-onion-constructed nanosheets (HCONs) from Co–hexamine coordination frameworks as high-performance potassium storage anode materials. However, all of the above hard templates require harmful acid solutions to etch away. NaCl templates avoid this problem by using water as the leaching solvent. Hence, Qiu and co-workers[59] prepared a N/P co-doped porous carbon (NPPC) by carbonizing the mixture of coal tar pitch and NaCl (Fig. 9c). As shown in Fig. 9d, NPPC has a pore structure composed of carbon sheets, which are distributed with a large number of mesopores of 10-30 nm. What's more, our group[60] reported the successful preparation of a hierarchical porous carbon (HPC) including micropores, mesopores and macropores by multiple templates (PAANa, NaCl and Zn nanoparticles). HPC benefits from the hierarchical porous structure that accelerates electrolyte penetration and K^+ migration rate, achieving an excellent rate performance (76.7 mAh g^{-1} at 10 A g^{-1}).

Different from the hard template method, the self-template with specific morphology is formed during the polymerization process without use of any additional templates[85]. Recently, Song's group[114] constructed carbon nanotube microspheres (CNTMs) by one step injected pyrolysis using thiophene and ferrocene as both catalysts and carbon sources. Qiu et al.[86] synthesized nitrogen-doped hierarchical porous hollow carbon spheres (NHCSs) by polymerization of 3-

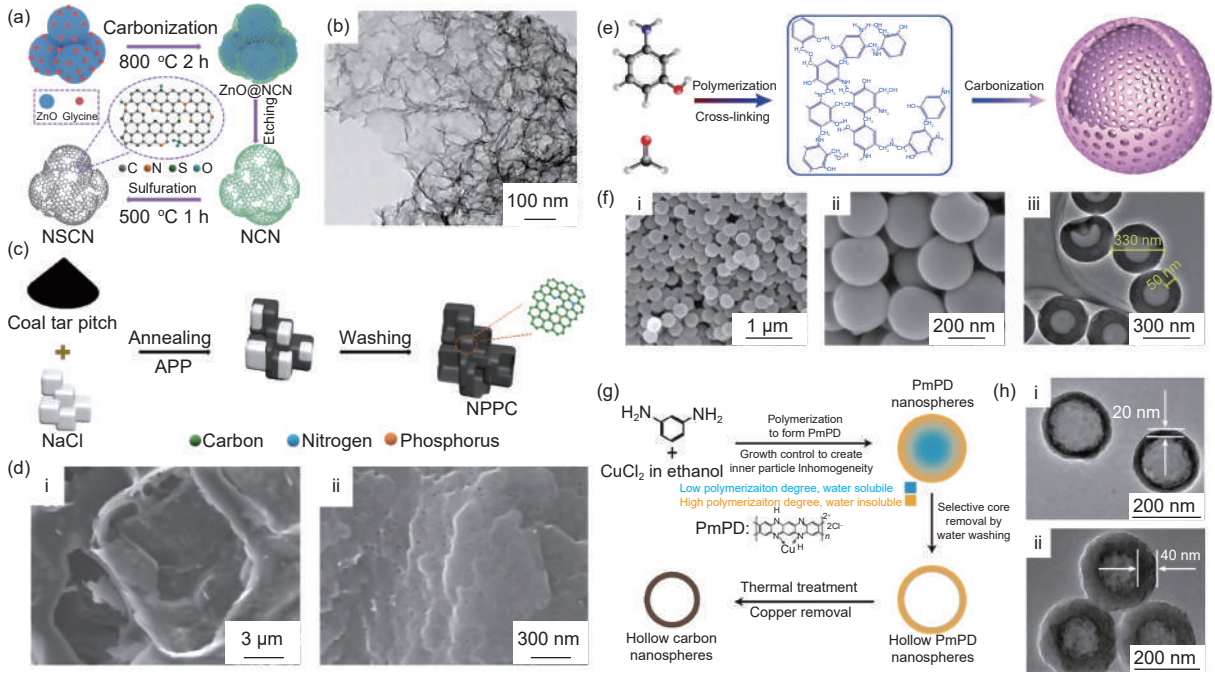

Fig. 9　(a) Schematic illustration of the synthesis process of NSCN. (b) SEM image of NSCN [36]. (c) Schematic illustration for the synthesis of NPPC. (d) (i) SEM and (ii) high-magnification SEM images of NPPC[59]. (e) Preparation principle of NHCS. (f) (i), (ii) SEM images, and (iii) TEM image of NHCS[86]. (g) Synthesis protocol for hollow carbon nanospheres. (h) TEM image of the hollow carbon spheres by reaction for (i) 20 min and (ii) 40 min[87](Reproduced with permission).

aminophenol with formaldehyde followed by carbonization (Fig. 9e). NHCSs exhibit a monodisperse hollow spherical shell structure, which possess an average diameter of about 330 nm and shell thickness of about 50 nm (Fig. 9f). Further, Tao et al.[87] developed hollow carbon nanospheres (HCNs) that have a controllable cavity size and shell thickness by a self-templating method (Fig. 9g). The morphology of the precursor and cavity size are adjusted by changing the polymerization reaction time and the solvent used for sample washing (Fig. 9h).

4.2 Heteroatom-doping

Currently, heteroatom-doping is mainly implemented through the direct pyrolysis of organic precursors containing heteroatoms or the reaction of carbon materials with substances containing heteroatoms at high temperatures. In addition, the post-annealing in NH_3, H_2S and other gases is also widely used due to their simplicity and controllability. Heteroatomic doping can increase the defect sites in carbon materials, thus providing more potassium storage active sites, which is an effective method to improve the electrochemical performance of carbon materials[88]. The doped elements mainly include non-metallic elements such as nitrogen, sulfur, boron and phosphorus.

Among them, N-doping is one of the main research directions, and the deep insights in the potassium storage mechanism of N-doped carbons have been gained. Share et al.[89] have demonstrated that N-doping in graphite can increase the potassium storage active sites between layers, boosting from a theoretical capacity of 278 to over 350 mAh g^{-1}. Moreover, most of the N-doped atoms are in the forms of pyridine N (N-6), pyridine N (N-5) and graphite N (N-Q), which are the different potassium storage sites[49]. Shen et al.[90] found that N-5 and N-6 can not only enhance the electrical conductivity but also increase the numbers of the defect sites and active sites. The adsorption energy (ΔE) of N-5 and N-6 are −2.63 and −2.86 eV, respectively as calculated by Discrete Fourier Transform DFT, which are much higher than that of N-Q (0.14 eV). This further indicates that the N-5 and N-6 dopings have significantly higher K^+ adsorption capacities than that of N-Q doping. On this basis, Zhang et al.[91] developed a highly nitrogen-doped (26.7 at.%) accordion-like carbon anode with a N-6 ratio of 48.4%, and a N-5 ratio of 43.7%. The results indicate that the dominant N-6 and N-5 dopings in anode materials lead to a high reversible capacity of 346 mAh g^{-1} and superior cycling stability. Moreover, Guo and co-works[92] reported the preparation of a single pyrrole nitrogen configuration doped carbon material (SPNCM) to provide a guide for investigating the energy storage mechanism of N-doped carbon materials. Electrochemical test results show that more pseudocapacitance can be delivered with increasing the single pyrrole nitrogen content.

The use of large radius heteroatoms such as S[61,93] and P[40,62] to expand the carbon layer spacing for K^+ storage has also been widely reported. Zheng et al.[61] expanded the carbon layer spacing from 0.37 to 0.38 nm by preparing sulfur-doped multichannel carbon fiber (S-MCCF) composites. S-MCCF possesses super-rate capability (exhibits 182.7 mAh g^{-1} at 2 A g^{-1}), and long-cycle stability (maintains 150 mAh g^{-1} after 2 000 cycles) as an anode material for PIBs. Furthermore, Li et al.[93] examined the storage mechanism of K^+ in S-doped carbon materials by *ex-situ* XPS at different charge/discharge depths during the first and second cycles. It is concluded that there is a strong binding force between C and S after doping. The C-S bond can react with K to form a C-S-K bond, which displays a K^+ storage capacity higher than of KC_8. By mixing red phosphorus with graphite, our group[62] successfully doped P into the carbon skeleton to form P-C and P-O-C bonds (Fig. 10a). As an anode material, both capacity (323.5 mAh g^{-1} at 0.05 A g^{-1}) (Fig. 10b) and rate performance (90 mAh g^{-1} at 0.5 A g^{-1}) (Fig. 10c) are enhanced as compared with a pure graphite electrode. On this basis, our group[40] further studied the effects of the chemical bonding states between P and carbon matrix on the K^+ storage performance (Fig. 10e) by compositing red phosphorus with different types of carbon nanotubes (Fig. 10d). Compared with the P-C bond (264 kJ mol^{-1}), the P-O-C bond (585 kJ mol^{-1}) dis-

plays a stronger binding energy. As a result, carbon anode with a P-O-C bond (P-CGCNT) performs an outstanding reversible capacity (402.6 mAh g^{-1} over 110 cycles at 0.1 A g^{-1}) (Fig. 10f) and excellent rate performance (258 mAh g^{-1} at 1 A g^{-1}) (Fig. 10g).

Due to the synergistic effect between two different heteroatoms, diatomic doping has also been shown to be a way of boosting the potassium storage performance for carbon anode materials[88,94]. Our group[39] produced a N/O co-doped graded porous carbon by carbonizing and acidizing the NH_2-MIL-101 (Al) precursor. Benefiting from the large layer spacing (0.39 nm), high SSA (1 030 m^2 g^{-1}) and abundant pores, the anode material delivers a high reversible capacities of 365 mAh g^{-1} at 25 mA g^{-1}. But from a commercial perspective, it is necessary to develop a cost-effective and manipulable strategy. In this regard, Cui et al.[95] realized a N/O self-doping hard carbon (NOHC) by simply carbonizing sorghum stalks. As a PIB anode material, NOHC exhibits a large average interlayer spacing (0.411 nm), enabling a high reversible capacity (304.6 mAh g^{-1} at 0.1 A g^{-1}) and superior cycle stability (189.5 mAh g^{-1} at 1 A g^{-1} after 5 000 cycles). In recent years, N/S doping has received increasing attention due to the fact that it can simultaneously obtain excellent conductivity and significantly enlarge the interlayer spacing[96]. Liu et al.[51] prepared N/S double-doping porous soft carbon nanosheets (NSC) using coal tar pitch, urea and sublimed sulfur as the carbon precursors, nitrogen source and sulfur source, respectively. N/S double doping boosts the interlayer distance, electronic conductivity and charge storage active sites (Fig. 11a). As a result, the NSC accomplishes a high capacity (359 mAh g^{-1} at 0.1 A g^{-1}), a high rate (115 mAh g^{-1} at 5.0 A g^{-1}) and a long cycle life (92.4% capacity retention after 1 000 cycles at 1.0 A g^{-1}). Moreover, our group[10] researched the effect of N and S elements on K^+ storage mechanism by *ex-situ* XPS (Fig. 11b, 11c). It is found that the content of N5 and N6 would gradually transform to NQ with increasing the pyrolysis temperature (Fig. 11b). N5 (*ca.* 398.5 eV) shows high activity at 600 °C, and the peak values of NQ-K (*ca.* 399.1 eV) and N6-K (*ca.* 398 eV) reach the maximum values at 1 000 °C. As shown in the S 2p XPS spectra (Fig. 11c), initial S $2p_{1/2}$ (165.0 eV) and S $2p_{3/2}$

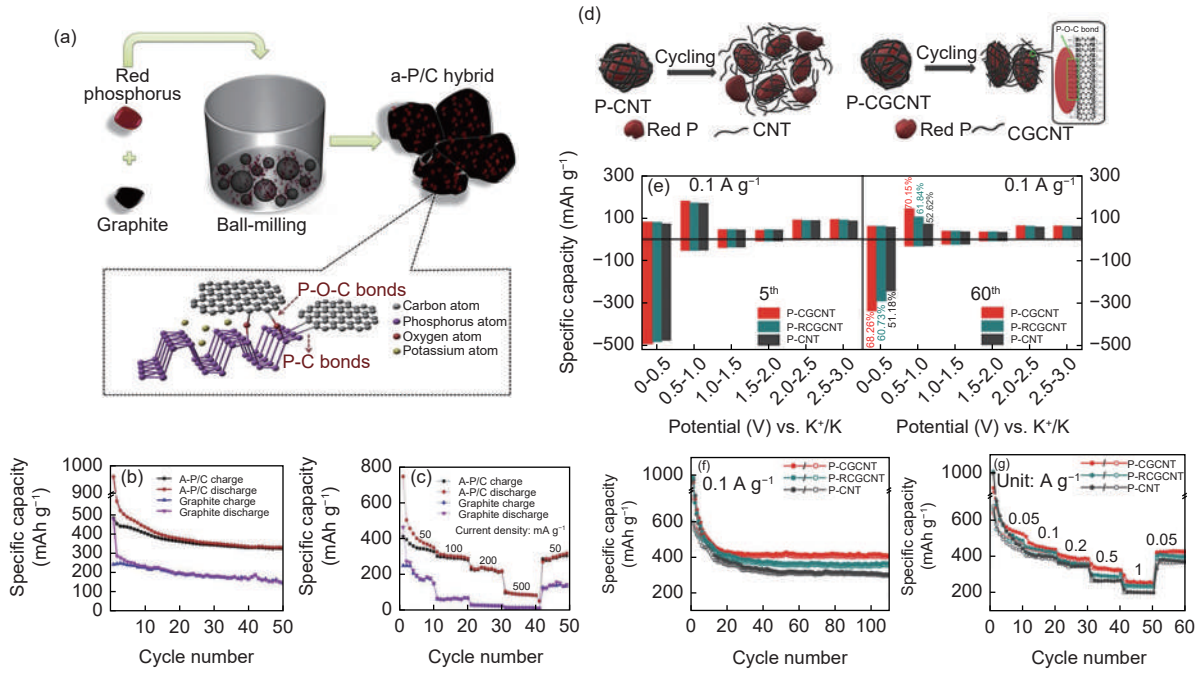

Fig. 10　(a) Schematic diagram of the synthesis of the P/C composite. (b) The cycling performance and (c) the rate performance of the P/C and pure graphite electrodes[62]. (d) Schematic illustration of the structure evolution of P-CNT and P-CGCNT electrodes during cycling. (e) The capacity retention in different voltage ranges of P-CGCNT and P-CNT electrodes at the 5th and 60th cycles. (f) The cycling performance and (g) the rate performance of P-CGCNT, P-RCGCNT, and P-CNT electrodes[40](Reproduced with permission).

(163.8 eV) are converted to new peaks related to -K_2S_x (162.5 and 161.5 eV) and thiosulfate/-K_2S_x (*ca.* 166.9 and 169.0 eV) during the discharge process. At the pyrolysis temperature of 1 000 °C, 66% of S is retained, in contrast to 600 and 800 °C where only 24% and 26% are retained during discharge and charge, respectively.

To sum up, various studies have shown that experimental parameters (such as the carbonization temperature) and heteroatomic precursors have a great influence on the content of the dopants. Generally speaking, the lower the carbonization temperature and the higher the heteroatomic content of the precursor, the higher the heteroatomic content of the products. At the same time, the type of heteroatom has a significant effect on K^+ storage performance. For example, Wang et al.[97] comprehensively compared the abilities of N, P and S dopants to capture K^+ in PIB anode materials by DFT calculation. Pyridine-N, pyrrole-N and P doping produce active sites in the carbon skeleton that are more inclined to capture K^+. However, both graphite-N and sulfur doping show poorer affinities to K^+.

4.3 Hybrid structure

Hybrid structures can enhance potassium storage performance by taking the advantage of different carbon structures. At present, many researches on carbon-based materials mainly focus on the sp^2-sp^3 hybrid structure: sp^2 hybrid carbon represented by graphite and graphene, and diamond and diamond-like sp^3 hybrid carbon. Our group[10] reported the successful preparation of sp^2-sp^3 hybrid carbon nanosheets (CNSs) by constructing an ordered graphite-like microcrystalline as conductive framework in defect-rich carbons (Fig. 12a, 12b). At low pyrolysis temperatures, massive heteroatom-defects are produced, providing active sites for K^+ storage, but resulting in many unstable sp^3 hybridization regions lack of elec-

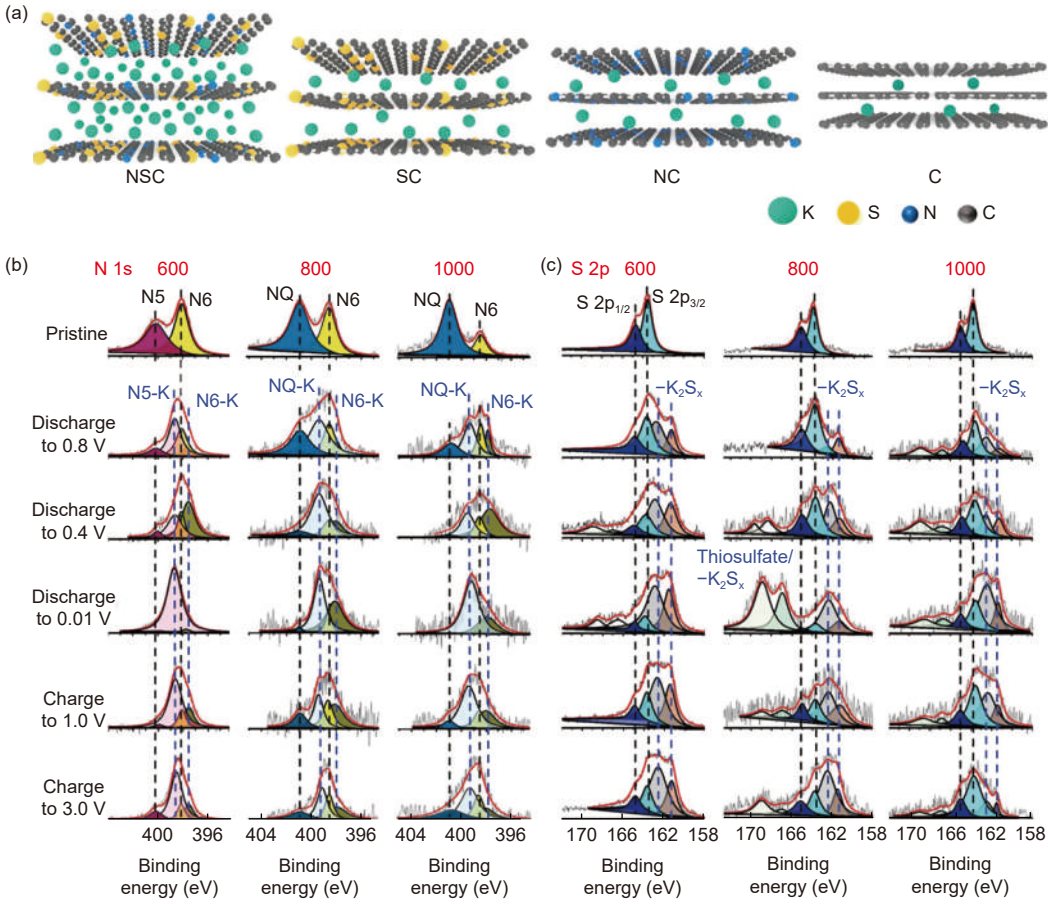

Fig. 11 (a) Schematic illustration of the carbon structures with different interlayer distances for the K^+ storage[51]. Deconvoluted (b) N 1s and (c) S 2p peaks of the electrodes[10](Reproduced with permission).

tron transport capability (Fig. 12c). By adjusting the pyrolysis temperature, the C atoms are selectively rearranged, which in turn constructs ordered graphite-like microcrystalline conducting skeletons in disordered defects (Fig. 12d). As shown in Fig. 12e, the TEM image clearly shows the "Order in Disorder" of the carbon structure in the carbon material. The sp^3 defect region is surrounded by the sp^2 nanographene network, which achieves fast charge transfer kinetics while ensuring sufficient K^+ storage sites (Fig. 12g). This sp^2-sp^3 hybridization region in CNS-1000 leads to superior rate capability (215 mAh g^{-1} at 2 A g^{-1}) (Fig. 12f) and long-term cyclic stability (maintain at 180.2 mAh g^{-1} after 5 000 cycles). In addition, Song's group has achieved a series of hybrid carbons by a simple ball milling method[98–100]. Ball milling leads to the introduction of mass self-doping defects in the graphene flakes and edges, which serve as active sites for ion adsorption and storage. The defect structures are distributed in the conductive network formed by the sp^2 carbon in the sp^2-sp^3 hybrid carbon. In conclusion, this sp^2-sp^3 hybrid structure not only provides abundant energy storage active sites for the anode material, but also exhibits good charge transfer capability due to the interconnected sp^2 pathways surrounding the sp^3 structure.

Moreover, the sp hybrid carbon attracts considerable attention owing to the good electrical conductivity and affinity for metal atoms as compared with the sp^2-sp^3 hybrid carbon[101]. In 2010, Li's group[102] synthesized graphdiyne, a new carbon allotrope, by a chemical method for the first time. This new material possesses sp, sp^2 and sp^3 hybrid structures and is promising for potassium storage. Sun and co-workers[103] determined the adsorption sites and transport paths of storage K^+ in graphdiyne (GDY) by DFT calculation. It is found that K^+ can not only migrate within layers but also shuttle vertically between layers. The theoretical capacity of GDY for potassium storage (620 mAh g^{-1}) is greatly increased compared to graphite (279 mAh g^{-1}). In addition, the GDY interlayer spacing can be expanded from *ca.* 0.37 to 0.41 nm by adjusting the annealing temperature to obtain superior rate performance (150 mAh g^{-1} at 5 A g^{-1}) and excellent cycling stability (over 90% after 2 000 cycles).

4.4 Composite structure

Composite materials, such as hard-soft carbon, graphite-soft carbon and graphite-hard carbon are promising for achieving the slope/plateau potassium storage. Wang and co-workers[63] synthesized the hard-soft carbon composite (Pi-700-P28) by carbonization of a mixture of polyimide and petroleum pitch at 700 °C (Fig. 13a). The XRD pattern in Fig. 13c exhibits that the Pi-700-P28 possesses good reversibility during charging/discharging. Moreover, *ex-situ* Ra-

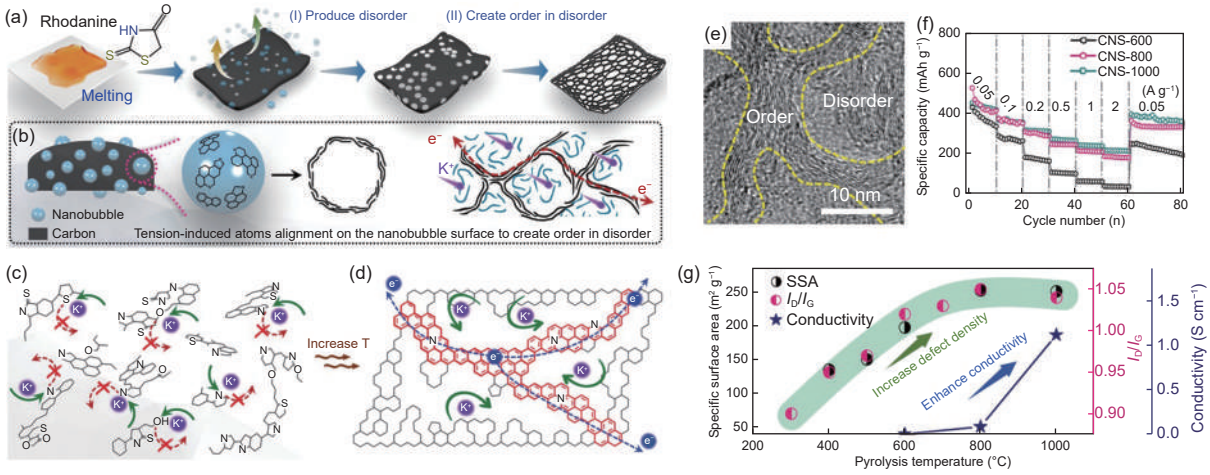

Fig. 12　(a) Schematic illustration of the construction of CNSs. (b) Schematic illustration of the alignment of carbon atoms on the nanobubble surface to create the order-in-disorder structure. Schematic illustration of the K^+ storage mechanism in CNSs obtained by (c) low and (d) high pyrolysis temperatures. (e) TEM images of CNS-1000. (f) Rate performance of CNS electrodes. (g) The variation of specific surface area, I_D/I_G and electric conductivity of CNSs with the pyrolysis temperature[10](Reproduced with permission).

man spectra (Fig. 13d, 13e) show a decrease in I_D/I_G from 1.44 to 1.29 during the potassiation process, indicating that K^+ is absorbed onto the material defects. As shown in Fig. 13b, potassium storage in graphite region is restricted due to edge accumulation and local bending of the graphite layer during K^+ intercalation/deintercalation. Benefiting from the hybrid potassium storage behavior, the hard-soft carbon composite performs a high initial reversible capacity of 376.8 mAh g^{-1} with an ICE of 71.04%. The (002) peak (Fig. 13g) and *G* peak (Fig. 13h) of G-SC 3∶1 has fewer positional shifts than graphite after full potassiation, indicating that the introduction of soft carbon shows a significant positive effect on the structural stability of graphite. As a result, G-SC 3∶1 manifests the highest ICE of 67.3% whereas those of graphite and SC are only 54.1% and 57.8%, respectively (Fig. 13f). Meanwhile, compositing graphite with hard carbon has also been shown to improve the electrochemical performance of anode materials. Graphite-hard carbon composites were formed by coating disordered carbon nanosheets on graphite, resulting in flat discharge voltage platform and excellent cycle stability (215.7 mAh g^{-1} after 1 000 cycles at 0.2 A g^{-1}) and ICE (61.83%)[29]. Obviously, the potassium storage mechanism can be adjusted by combining different types of precursors to obtain a balanced performance of a carbon material with a high capacity, high ICE and good cycling stability.

5 Full device performance

The assembly of full device is particularly important in achieving the practical application of the anode material. Moreover, it is essential to guide the full device fabrication based on the structural and electrochemical relationships of the anode materials. Potassium storage devices can be divided into two types in full devices: potassium ion batteries (PIBs) and potassium ion hybrid capacitors (PIHCs). Here,

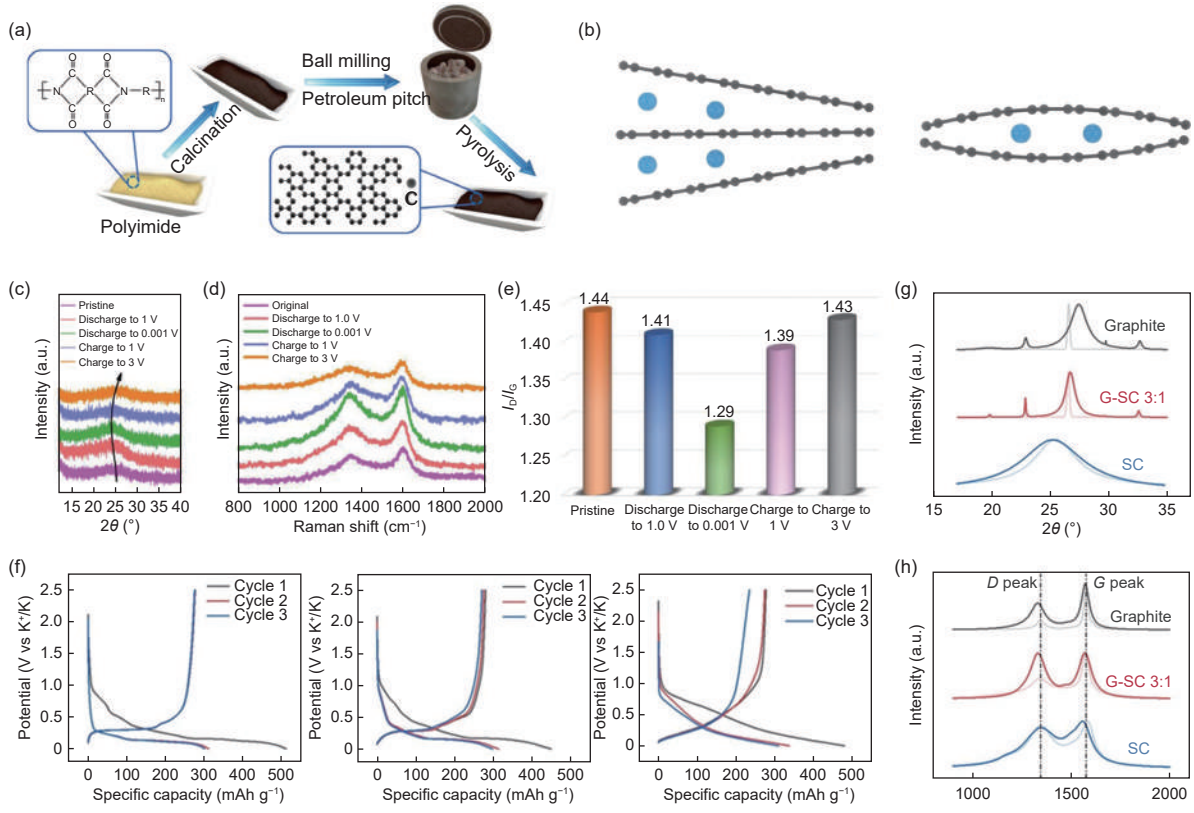

Fig. 13 (a) Schematic illustration of the preparation of the hard-soft carbon composites[63]. (b) Unfavorable intercalation with accumulated K^+ at one edge of graphite and local bending of the graphite layer locking K^+[28]. (c) Ex-situ XRD patterns and (d) Raman spectra of PI-700-P28 electrode at typical charge/discharge stages and their pristine states. (e) I_D/I_G ratios of PI-700-P28 electrode at different charge/discharge states. (f) GCD curves at 0.1 C of *G* (left), G-SC 3∶1 (middle) and SC (right). (g) *Ex-situ* XRD patterns of G, G-SC 3∶1 and SC. (h) *Ex-situ* Raman spectra of G, G-SC 3∶1 and SC (Reproduced with permission).

we introduce the anode materials of the two potassium storage devices.

PIBs usually use carbonaceous materials (graphite, soft carbon, hard carbon, etc.) as the anode materials and K-containing compounds (Prussian blue analogs, layered metal oxides, polyanionic compounds, and organic crystals) as the cathode materials[104]. During charging, K^+ is extracted from the cathode into the electrolyte and migrates to the anode for intercalating. Correspondingly, K^+ inserted in the anode are extracted and reinserted into the cathode during discharge[105]. Lu's group[69] assembled a graphite/perylene-3, 4,9,10-tetracarboxylic dianhydride (PTCDA) full cell using a concentrated electrolyte (KFSI: EMC, 1∶2.5, molar ratio) (Fig. 14a). Graphite/PTCDA delivers a cyclic stability of 92.9 % capacity retention after 50 cycles at 30 mA g^{-1} (Fig. 14b) and a high-rate capability (from 80 mAh g^{-1} at 10 mA g^{-1} to 74 mAh g^{-1} at 60 mA g^{-1}) (Fig. 14c), based on the active materials in both anode and cathode. Similarly, Qin et al.[106] assembled a potassium ion full cell by matching the graphite anode with the potassium Prussian blue (KPB) cathode in a highly concentrated electrolyte (KFSI∶DME∶HFE, 1∶1.9∶0.95, molar ratio). The full cell shows a distinct voltage plateau in the voltage range of 2.0-4.0 V, achieving a high CE of 99.7% after 100 cycles. Xu et al.[49] reported a full cell coupling of the soft carbon (carbon nanofibers) anode and KPB cathode. The soft carbon/KPB full cell is tested in a voltage window of 2.0-4.2 V, showing an initial discharge capacity of 197 mAh g^{-1} (based on the anode mass) and a 97% capacity retention (190 mAh g^{-1}) after 30 cycles at 0.2 A g^{-1}. Our group[10] assembled a hard carbon/KPB full cell using carbon nanosheets and KPB as the anode and cathode, respectively (Fig. 14d). The CE of the full cell re-

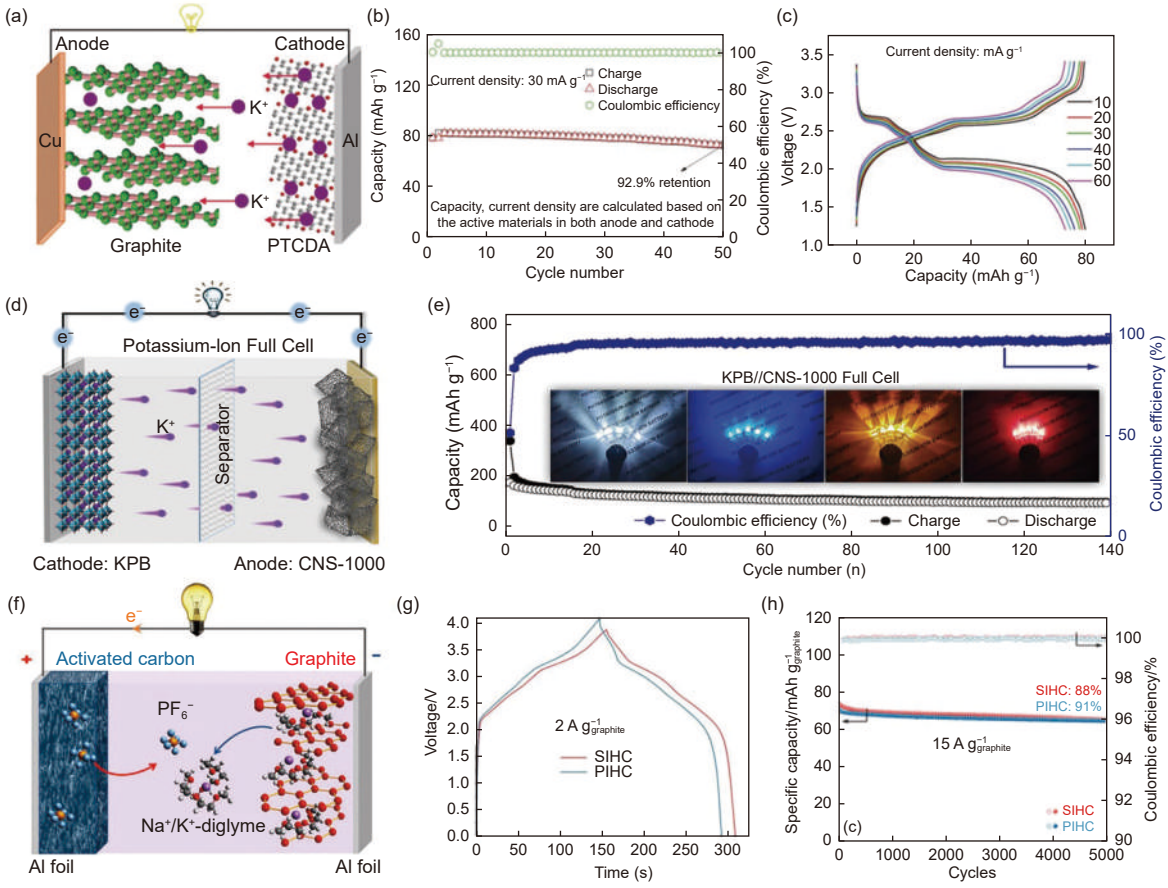

Fig. 14　Potassium-ion full cell and potassium-ion hybrid capacitor based on the carbon electrode. (a) Schematic illustration of the graphite/PTCDA full cell. (b) Cycle stability at 30 mA g^{-1}. (c) Charge/discharge curves at different current densities[69]. (d) Schematic illustration of the hard carbon/KPB full-cell. (e) The long cycle performance of the full cell at 0.1 A g^{-1}[10]. (f) Schematic illustration for the working mechanism of PIHC. (g) Charge/discharge curves at 2 A g^{-1} and (h) prolonged cycling of the PIHC[111](Reproduced with permission).

mains above 96% after 20 cycles and the LED bulbs can be lit normally, indicating that the HC/KPB full cell works stably (Fig. 14e). Furthermore, replacing toxic metal compounds with graphite as cathode for potassium dual-ion batteries (PDIB)[107–110] has potential applications due to the fact that both of them are environmentally friendly and cost-effective carbon materials.

Potassium ion hybrid capacitors (PIHC) have attracted widespread attention because of the advantages of high energy density, high power and long cycle life compared to PIBs. Dual carbon PIHCs (DC-PIHCs), in which both electrodes are composed of carbon materials, have been studied in activated carbon (AC) cathodes and various anodes (graphite, soft carbon, hard carbon, etc.). Graphite/AC PIHC was assembled with graphite as the anode for K^+ intercalation/deintercalation and AC as the cathode for K^+ adsorption/desorption. Passerini and co-workers[111] reported graphite/AC PIHC and sodium ion hybrid capacitor (SIHC) (Fig. 14f). The charge-discharge curves display a higher voltage plateau than conventional capacitors, resulting in higher energy density and power density (Fig. 14g). Fig. 14h shows the excellent cycling stability of graphite/AC PIHC and SIHC, which maintain 91% and 88% of initial capacity at 15 A g^{-1} (based on graphite mass) after 5 000 cycles, respectively. Fan et al.[112] established a PIHC using a soft carbon as the anode and an AC as the cathode, which displays excellent energy density (120 Wh kg^{-1}) and power density (599 W kg^{-1}). To enhance the capacitive behavior of PIHC anode materials, more efforts are focused on the structural modification of soft carbon materials. Recently, Wu and co-workers[113] developed a novel accordion-like soft carbon structure with a hierarchical porous framework consisting of micro-, meso-, and macro-pores. Furthermore, the pseudocapacitance of the anode material is improved by electrodeposition to form nitrogen-doped graphene quantum dots. Ultimately, the PIHC is obtained by matching with a porous carbon (PC) cathode, achieving a superhigh energy and power density (171 Wh kg^{-1} and 20 000 W kg^{-1}). When a PIHC is designed, the hard carbon anode can provide high power density and superior cycling performance due to amorphous structures with large interlayer distances and high defect density. Cao et al.[44] assembled the PIHC using hard carbon as the anode and PC as the cathode, which manifests ultrahigh cycle performance (89.2% capacity retention after 6 000 cycles) and high energy/power density (120.2 Wh kg^{-1} and 16 700 W kg^{-1}).

In summary, the intercalation-dominated carbon materials can be designed as anode materials for potassium ion full cells, which is ascribed to the low and stable intercalation potential platform that can provide a high energy density and stable working conditions for potassium ion full cells. In contrast, carbon materials with surface-driven K^+ storage mechanism are more suitable for the development of anode materials for high power density potassium ion capacitors due to their faster ion transport and more active sites.

6 Conclusion and perspectives

At present, carbons are considered as important potassium storage materials due to their advantages of low cost, good electrical conductivity, controlled surface chemistry and structure. From the recent progress of various carbon materials in PIBs, it is found that the potassium storage capacity of the carbon materials is mainly related to K^+ transfer, electron transport and active sites. In this review, we introduced the effects of different active sites on potassium storage mechanisms. Graphite and graphite-like materials are dominated by K^+ interlayer storage with low potential plateaus. However, the serious volume expansion and kinetic hysteresis in graphite material result in poor cycle stability, capacity fading and low-rate performance. Soft carbon with a turbostratic structure can enhance K^+ adsorption at the edge of carbon sheets, which alleviates structural instability during the charging and discharging. In addition, soft carbon can be converted to graphite after annealing at temperatures higher than 2 500 °C, which is valuable for studying the relationship between carbon structure and electrochemical properties due to structure tuning by the annealing temperature. Hard carbon with abundant carbon defects and large SSA boosts the surface-driven

K^+ adsorption, leading to high capacity and excellent rate performance. However, the low ICE and the sloping curve limit their practical applications. Therefore, it is essential to consider the trade-off between intercalation and surface-driven mechanisms when carbon structures are designed.

On this basis, we have systematically discussed the rational design strategies of carbon anodes such as heteroatom doping, pore generation and hybridization of sp, sp^2 and sp^3. The introduction of pore structures in carbon materials can increase the surface area, accelerate the electrode/electrolyte contact, and shorten the diffusion distance of ions/electrons. Heteroatom doping can enhance the defective sites within the carbon material, thus providing more active sites for energy storage. It is found that the co-doping of different heteroatoms could improve the electrochemical properties of carbon anode materials by synergistic effects. Hybrid carbon materials possess excellent potassium storage performance through the combination of sp, sp^2 and sp^3 carbons. The composite structure can adjust the K^+ storage mechanism by combining different types of precursors, resulting in anode materials with balanced potassium storage properties. Moreover, the assembly of potassium storage full devices is reviewed according to the structure and electrochemical relationship of advanced anode materials.

Despite considerable progress has been made to date, the following challenges and opportunities may exist as the researches on carbon-based anodes progress.

(1) When advanced carbon anode materials are designed, the comprehensive properties of potassium storage should be considered. The research of electrochemical potassium storage in carbon materials is mainly in two directions: low potential and high capacity/high rate. The existing carbon anode materials have problems in balancing low potential potassium storage and high capacity/high rate performance, and further development is needed to optimize the carbon structure.

(2) Graphite has been attracting much attention as the most mature anode electrode for commercial batteries. However, the intercalating of large radius K^+ causes the collapse of the graphite structure during cycling. In order to improve the electrochemical properties of graphite in K^+ storage, many efforts have been made such as electrolyte development, electrolyte formulation optimization and morphology design of electrodes. Yet the cycle stability of the optimized graphite anode still does not meet the requirements for practical applications.

(3) For PIBs, the mechanisms of potassium storage in graphite and soft carbon have been well investigated. However, the complexity and uncertainty of the hard carbon structure result in controversy of the electrochemical mechanism, which requires further studies on the storage behavior of K^+ in hard carbon. In addition, the control of graphitized microdomains, defects and nanopores in hard carbon is critically important for potassium storage. Thus, it is urgent to understand the relevant mechanism driving the rational design of hard carbon.

(4) In the implementation of the whole device, the anode and cathode need to be matched thermodynamically and kinetically. Moreover, a clear understanding of the reaction mechanism for the electrodes is required to give full play to the high-performance potassium storage advantages of the electrode materials. And the mass of the electrode materials needs to be carefully calculated and matched.

Acknowledgements

This research was supported by the National Natural Science Foundation of China (21975283), China Postdoctoral Science Foundation (2020M681762), State Key Laboratory of Chemistry and Utilization of Carbon-based Energy Resource (KFKT2021007), and CAS Key Laboratory of Carbon Materials (KLCMK-FJJ2010).

References

[1] Wu Y M, Zhao H T, Wu Z G, et al. Rational design of carbon materials as anodes for potassium-ion batteries[J]. Energy Storage Materials, 2021, 34: 483-507.

[2] Guo R, Liu X, Wen B, et al. Engineering mesoporous structure in amorphous carbon boosts potassium storage with high initial coulombic efficiency[J]. Nano-Micro Letters, 2020, 12(1): 148.

[3] Zhu C Y, Ye Y W, Guo X, et al. Design and synthesis of carbon-

based nanomaterials for electrochemical energy storage[J]. New Carbon Materials, 2022, 37(1): 59-92.
[4] Shaker M, Ghazvini A A S, Cao W Q, et al. Biomass-derived porous carbons as supercapacitor electrodes - A review[J]. New Carbon Materials, 2021, 36(3): 546-572.
[5] Sepulveda N A, Jenkins J D, Edington A, et al. The design space for long-duration energy storage in decarbonized power systems[J]. Nature Energy, 2021, 6(5): 506-516.
[6] Chen Y X, Shi L L, Yuan Q, et al. Crystallization-induced morphological tuning toward denim-like graphene nanosheets in a KCl-copolymer solution[J]. ACS Nano, 2018, 12(4): 4019-4024.
[7] Wu X, Chen Y X, Xing Z, et al. Advanced carbon - based anodes for potassium - ion batteries[J]. Advanced Energy Materials, 2019, 9(21): 1900343.
[8] Wang D K, Zhang J P, Dong Y, et al. Progress on graphitic carbon materials for potassium-based energy storage[J]. New Carbon Materials, 2021, 36(3): 435-448.
[9] Ju Z C, Li P Z, Ma G Y, et al. Few layer nitrogen-doped graphene with highly reversible potassium storage[J]. Energy Storage Materials, 2018, 11: 38-46.
[10] Chen Y X, Xi B J, Huang M, et al. Defect-selectivity and "order in disorder" engineering in carbon for durable and fast potassium storage[J]. Advanced Materials, 2021, 34(7): 2108621.
[11] Rajagopalan R, Tang Y, Ji X, et al. Advancements and challenges in potassium ion batteries: A comprehensive review[J]. Advanced Functional Materials, 2020, 30(12): 1909486.
[12] Lei K X, Li F J, Mu C N, et al. High K-storage performance based on the synergy of dipotassium terephthalate and ether-based electrolytes[J]. Energy & Environmental Science, 2017, 10(2): 552-557.
[13] Kubota K, Dahbi M, Hosaka T, et al. Towards K-ion and Na-ion batteries as "beyond Li-ion"[J]. Chemical record (New York, N.Y.), 2018, 18(4): 459-479.
[14] Zhang L P, Wang W, Lu S F, et al. Carbon anode materials: A detailed comparison between Na - ion and K - ion batteries[J]. Advanced Energy Materials, 2021, 11(11): 2003640.
[15] Gao F, Zang Y H, Wang Y, et al. A review of the synthesis of carbon materials for energy storage from biomass and coal/heavy oil waste[J]. New Carbon Materials, 2021, 36(1): 34-48.
[16] Tan H, Du X Q, Zhou R, et al. Rational design of microstructure and interphase enables high-capacity and long-life carbon anodes for potassium ion batteries[J]. Carbon, 2021, 176: 383-389.
[17] Liu S, Kang L, Zhang J, et al. Carbonaceous anode materials for non-aqueous sodium- and potassium-ion hybrid capacitors[J]. ACS Energy Letters, 2021, 6(11): 4127-4154.
[18] Zhang J, Lai L, Wang H, et al. Energy storage mechanisms of anode materials for potassium ion batteries[J]. Materials Today Energy, 2021, 21: 100747.
[19] Wu S, Song Y, Lu C, et al. An adsorption-insertion mechanism of potassium in soft carbon[J]. Small, 2021, 18(4): 2105275.
[20] Chen J F, Feng J M, Dong L, et al. Nanoporous coal via Ni-catalytic graphitization as anode materials for potassium ion battery[J]. Journal of Electroanalytical Chemistry, 2020, 862: 113902.
[21] Du J C, Gao S S, Shi P H, et al. Three-dimensional carbonaceous for potassium ion batteries anode to boost rate and cycle life performance[J]. Journal of Power Sources, 2020, 451: 227727.
[22] Zhang W C, Liu Y J, Guo Z P, et al. Approaching high-performance potassium-ion batteries via advanced design strategies and engineering[J]. Science Advances, 2019, 5(5): eaav7412.
[23] Yin B, Liang S, Yu D, et al. Increasing accessible subsurface to improving rate capability and cycling stability of sodium-ion batteries[J]. Advanced Materials, 2021, 33(37): 2100808.
[24] Liu Z, Zhang L H, Sheng L Z, et al. Edge-nitrogen-rich carbon dots pillared graphene blocks with ultrahigh volumetric/gravimetric capacities and ultralong life for sodium-ion storage[J]. Advanced Energy Materials, 2018, 8(30): 1802042.
[25] Liu L Y, Lin Z F, Chane-Ching J Y, et al. 3D rGO aerogel with superior electrochemical performance for K –ion battery[J]. Energy Storage Materials, 2019, 19: 306-313.
[26] An Y L, Fei H F, Zeng G F, et al. Commercial expanded graphite as a low–cost, long-cycling life anode for potassium–ion batteries with conventional carbonate electrolyte[J]. Journal of Power Sources, 2018, 378: 66-72.
[27] Sultana I, Rahman M M, Ramireddy T, et al. High capacity potassium-ion battery anodes based on black phosphorus[J]. Journal of Materials Chemistry A, 2017, 5(45): 23506-23512.
[28] Zhang S, Teck A A, Guo Z Y, et al. Carbon composite anodes with tunable microstructures for potassium - ion batteries[J]. Batteries & Supercaps, 2021, 4(4): 663-670.
[29] Tian S, Zhang Y, Yang C H, et al. Nitrogen-doped carbon nanosheet coated multilayer graphite as stabilized anode material of potassium-ion batteries with high performances[J]. Electrochimica Acta, 2021, 380: 138254.
[30] Xu S, Cai L, Niu P, et al. The creation of extra storage capacity in nitrogen-doped porous carbon as high-stable potassium-ion battery anodes[J]. Carbon, 2021, 178: 256-264.
[31] Yu F, Huang T, Zhang P P, et al. Design and synthesis of electrode materials with both battery-type and capacitive charge storage[J]. Energy Storage Materials, 2019, 22: 235-255.
[32] Zhang Y, Tao L, Xie C, et al. Defect engineering on electrode materials for rechargeable batteries[J]. Advanced Materials, 2020, 32(7): 1905923.
[33] Wu J, Zhang X X, Li Z, et al. Toward high - performance capacitive potassium - ion storage: A superior anode material from silicon carbide - derived carbon with a well - developed pore structure[J]. Advanced Functional Materials, 2020, 30(40): 2004348.
[34] Chen Y X, Shi L L, Li A, et al. Capacity enhancement of porous carbon electrodes during long-term cycling in lithium-ion batteries[J]. Journal of The Electrochemical Society, 2017, 164(9): 2000-A2006.
[35] Chen Y X, Shi L L, Guo S S, et al. A general strategy towards carbon nanosheets from triblock polymers as high-rate anode materials for lithium and sodium ion batteries[J]. Journal of Materials Chemistry A, 2017, 5(37): 19866-19874.
[36] Bi H H, He X J, Yang L, et al. Interconnected carbon

nanocapsules with high N/S co-doping as stable and high-capacity potassium-ion battery anode[J]. Journal of Energy Chemistry, 2022, 66: 195-204.

[37] Chen Y, Shi L, Li D, et al. Undercooling-directed nacl crystallization: An approach towards nanocavity-linked graphene networks for fast lithium and sodium storage[J]. Nanoscale, 2020, 12(14): 7622-7630.

[38] Guo Y Y, Feng Y F, Li H, et al. Carbon quantum dots in hard carbon: an approach to achieving PIB anodes with high potassium adsorption[J]. Carbon, 2022, 189(15): 142-151.

[39] Yang J, Ju Z, Jiang Y, et al. Enhanced capacity and rate capability of nitrogen/oxygen dual-doped hard carbon in capacitive potassium-ion storage[J]. Advanced Materials, 2018, 30(4): 1700104.

[40] Peng D Q, Chen Y X, Ma H L, et al. Enhancing the cycling stability by tuning the chemical bonding between phosphorus and carbon nanotubes for potassium-ion battery anodes[J]. ACS Applied Materials & Interfaces, 2020, 12(33): 37275-37284.

[41] Zhang W C, Lu J Guo Z P. Challenges and future perspectives on sodium and potassium ion batteries for grid-scale energy storage[J]. Materials Today, 2021, 50: 400-417.

[42] Wang B, Peng Y, Yuan F, et al. A comprehensive review of carbons anode for potassium-ion battery: Fast kinetic, structure stability and electrochemical[J]. Journal of Power Sources, 2021, 484: 229244.

[43] Jiang Y, Yang Y, Xu R, et al. Ultrafast potassium storage in F-induced ultra-high edge-defective carbon nanosheets[J]. ACS Nano, 2021, 15(6): 10217-10227.

[44] Liu H, Du H L, Zhao W, et al. Fast potassium migration in mesoporous carbon with ultrathin framework boosting superior rate performance for high-power potassium storage[J]. Energy Storage Materials, 2021, 40: 490-498.

[45] Jian Z, Luo W, Ji X. Carbon electrodes for K-ion batteries[J]. Journal of the American Chemical Society, 2015, 137(36): 11566-9.

[46] Wang B, Gu L, Yuan F, et al. Edge-enrich N-doped graphitic carbon: Boosting rate capability and cyclability for potassium ion battery[J]. Chemical Engineering Journal, 2022, 432(15): 134321.

[47] Xing Z, Qi Y, Jian Z, et al. Polynanocrystalline graphite: A new carbon anode with superior cycling performance for K-ion batteries[J]. ACS Applied Materials & Interfaces, 2017, 9(5): 4343-4351.

[48] Hosaka T, Kubota K, Kojima H, et al. Highly concentrated electrolyte solutions for 4 V class potassium-ion batteries[J]. Chemical Communications, 2018, 54(60): 8387-8390.

[49] Xu Y, Zhang C, Zhou M, et al. Highly nitrogen doped carbon nanofibers with superior rate capability and cyclability for potassium ion batteries[J]. Nature Communications, 2018, 9(1): 1720.

[50] Liu C, Xiao N, Li H J, et al. Nitrogen-doped soft carbon frameworks built of well-interconnected nanocapsules enabling a superior potassium-ion batteries anode[J]. Chemical Engineering Journal, 2020, 382(15): 121759.

[51] Liu Q, Han F, Zhou J, et al. Boosting the potassium-ion storage performance in soft carbon anodes by the synergistic effect of optimized molten salt medium and N/S dual-doping[J]. ACS Applied Materials & Interfaces, 2020, 12(18): 20838-20848.

[52] Liu Y, Lu Y X, Xu Y S, et al. Pitch-derived soft carbon as stable anode material for potassium ion batteries[J]. Advanced Materials, 2020, 32(17): 2000505.

[53] Tan H, Zhou R Zhang B. Understanding potassium ion storage mechanism in pitch-derived soft carbon and the consequence on cyclic stability[J]. Journal of Power Sources, 2021, 506: 230179.

[54] Wang P F, Gong Z, Ye K, et al. N-rich biomass carbon derived from hemp as a full carbon-based potassium ion hybrid capacitor anode[J]. Applied Surface Science, 2021, 553: 149569.

[55] Liu Y, Dai H D, Wu L, et al. A large scalable and low - cost sulfur/nitrogen dual - doped hard carbon as the negative electrode material for high - performance potassium - ion batteries[J]. Advanced Energy Materials, 2019, 9(34): 1901379.

[56] Tao S, Xu W, Zheng J H, et al. Soybean roots-derived N, P co-doped mesoporous hard carbon for boosting sodium and potassium-ion batteries[J]. Carbon, 2021, 178: 233-242.

[57] Li W Z, Zhang R, Chen Z, et al. Microstructure-dependent K^+ storage in porous hard carbon[J]. Small, 2021, 17(21): 2100397.

[58] Yuan F, Zhang D, Li Z, et al. Unraveling the intercorrelation between micro/mesopores and K migration behavior in hard carbon [J]. Small, 2022, 18 (12): 2107113. DOI: 10.1002/smll.202107113.

[59] Ma X Q, Xiao N, Xiao J, et al. Nitrogen and phosphorus dual-doped porous carbons for high-rate potassium ion batteries[J]. Carbon, 2021, 179: 33-41.

[60] Wu X, Lam C W K, Wu N Q, et al. Multiple templates fabrication of hierarchical porous carbon for enhanced rate capability in potassium-ion batteries[J]. Materials Today Energy, 2019, 11: 182-191.

[61] Xu Y, Ruan J, Pang Y, et al. Homologous strategy to construct high-performance coupling electrodes for advanced potassium-ion hybrid capacitors[J]. Nano-Micro Letters, 2020, 13(1): 14.

[62] Wu X, Zhao W, Wang H, et al. Enhanced capacity of chemically bonded phosphorus/carbon composite as an anode material for potassium-ion batteries[J]. Journal of Power Sources, 2018, 378: 460-467.

[63] Wang M Y, Zhu Y Y, Zhang Y, et al. Cost-effective hard–soft carbon composite anodes with promising potassium ions storage performance[J]. Electrochimica Acta, 2021, 368: 137649.

[64] Cao B, Zhang Q, Liu H, et al. Graphitic carbon nanocage as a stable and high power anode for potassium-ion batteries[J]. Advanced Energy Materials, 2021, 8(25): 1801149.

[65] Tai Z X, Zhang Q, Liu Y J, et al. Activated carbon from the graphite with increased rate capability for the potassium ion battery[J]. Carbon, 2017, 123: 54-61.

[66] Liu Z, Wang J, Jia X, et al. Graphene armored with a crystal carbon shell for ultrahigh-performance potassium ion batteries and aluminum batteries[J]. ACS Nano, 2019, 13(9): 10631-10642.

[67] Lin X Y, Huang J Q, Zhang B. Correlation between the microstructure of carbon materials and their potassium ion storage

performance[J]. Carbon, 2019, 143: 138-146.

[68] Zeng S, Zhou X F, Wang B, et al. Freestanding CNT-modified graphitic carbon foam as a flexible anode for potassium ion batteries[J]. Journal of Materials Chemistry A, 2019, 7(26): 15774-15781.

[69] Fan L, Ma R, Zhang Q, et al. Graphite anode for a potassium-ion battery with unprecedented performance[J]. Angewandte Chemie International Edition, 2019, 58(31): 10500-10505.

[70] Wang H H, Yang G, Chen Z, et al. Nitrogen configuration dependent holey active sites toward enhanced K^+ storage in graphite foam[J]. Journal of Power Sources, 2019, 419: 82-90.

[71] Shen Y P, Huang C, Li Y H, et al. Enhanced sodium and potassium ions storage of soft carbon by a S/O co-doped strategy[J]. Electrochimica Acta, 2021, 367: 137526.

[72] Ou M Y, Zhang Y, Zhu Y, et al. Local structures of soft carbon and electrochemical performance of potassium-ion batteries[J]. ACS Applied Materials & Interfaces, 2021, 13(24): 28261-28269.

[73] Kubota K, Shimadzu S, Yabuuchi N, et al. Structural analysis of sucrose-derived hard carbon and correlation with the electrochemical properties for lithium, sodium, and potassium insertion[J]. Chemistry of Materials, 2020, 32(7): 2961-2977.

[74] Chen C, Wu M Q, Wang Y S, et al. Insights into pseudographite-structured hard carbon with stabilized performance for high energy K-ion storage[J]. Journal of Power Sources, 2019, 444: 227310.

[75] Alvin S, Cahyadi H S, Hwang J, et al. Revealing the intercalation mechanisms of lithium, sodium, and potassium in hard carbon[J]. Advanced Energy Materials, 2020, 10(20): 2000283.

[76] Wang B, Zhang Z Y, Yuan F, et al. An insight into the initial coulombic efficiency of carbon-based anode materials for potassium-ion batteries[J]. Chemical Engineering Journal, 2022, 428: 131093.

[77] Zhang H H, Luo C, He H N, et al. Nano-size porous carbon spheres as a high-capacity anode with high initial coulombic efficiency for potassium-ion batteries[J]. Nanoscale Horizons, 2020, 5(5): 895-903.

[78] Xu Y S, Duan S Y, Sun Y G, et al. Recent developments in electrode materials for potassium-ion batteries[J]. Journal of Materials Chemistry A, 2019, 7(9): 4334-4352.

[79] Chen J C, Xiao G C, Duan G G, et al. Structural design of carbon dots/porous materials composites and their applications[J]. Chemical Engineering Journal, 2021, 421(1): 127743.

[80] Zhu J W, Mu S C. Defect engineering in carbon - based electrocatalysts: Insight into intrinsic carbon defects[J]. Advanced Functional Materials, 2020, 30(25): 2001097.

[81] Li J P, Li Y J, Ma X D, et al. A honeycomb-like nitrogen-doped carbon as high-performance anode for potassium-ion batteries[J]. Chemical Engineering Journal, 2020, 384(15): 123328.

[82] Liu S T, Yang B B, Zhou J S, et al. Nitrogen-rich carbon-onion-constructed nanosheets: an ultrafast and ultrastable dual anode material for sodium and potassium storage[J]. Journal of Materials Chemistry A, 2019, 7(31): 18499-18509.

[83] Benzigar M R, Talapaneni S N, Joseph S, et al. Recent advances in functionalized micro and mesoporous carbon materials: synthesis and applications[J]. Chemical Society Reviews, 2018, 47(8): 2680-2721.

[84] Lee J, Oh J, Jeon Y, et al. Multi-heteroatom-doped hollow carbon attached on graphene using $LiFePO_4$ nanoparticles as hard templates for high-performance lithium-sulfur batteries[J]. ACS Applied Materials & Interfaces, 2018, 10(31): 26485-26493.

[85] Wang W K, Zhao W W, Chen T T, et al. All - in - one hollow flower - like covalent organic frameworks for flexible transparent devices[J]. Advanced Functional Materials, 2021, 31(29): 2010306.

[86] Qiu D P, Guan J Y, Li M, et al. Kinetics enhanced nitrogen - doped hierarchical porous hollow carbon spheres boosting advanced potassium - ion hybrid capacitors[J]. Advanced Functional Materials, 2019, 29(32): 1903496.

[87] Tao X S, Sun Y G, Liu Y, et al. Facile synthesis of hollow carbon nanospheres and their potential as stable anode materials in potassium-ion batteries[J]. ACS Applied Materials & Interfaces, 2020, 12(11): 13182-13188.

[88] Lin Q, Zhang J, Lv W, et al. A functionalized carbon surface for high-performance sodium-ion storage[J]. Small, 2020, 16(15): 1902603.

[89] Share K, Cohn A P, Carter R, et al. Role of nitrogen-doped graphene for improved high-capacity potassium ion battery anodes[J]. ACS Nano, 2016, 10(10): 9738-9744.

[90] Shen W, Wang C, Xu Q J, et al. Nitrogen-doping-induced defects of a carbon coating layer facilitate Na-storage in electrode materials[J]. Advanced Energy Materials, 2015, 5(1): 1400982.

[91] Zhang W L, Sun M L, Yin J, et al. Accordion-like carbon with high nitrogen doping for fastand stable K ion storage[J]. Advanced Energy Materials, 2021, 11(41): 2101928.

[92] Tian K, Wang J, Cao L, et al. Single-site pyrrolic-nitrogen-doped sp^2-hybridized carbon materials and their pseudocapacitance[J]. Nature Communications, 2020, 11(1): 3884.

[93] Li J L, Qin W, Xie J P, et al. Sulphur-doped reduced graphene oxide sponges as high-performance free-standing anodes for K-ion storage[J]. Nano Energy, 2018, 53: 415-424.

[94] Chen W M, Wan M, Liu Q, et al. Heteroatom - doped carbon materials: synthesis, mechanism, and application for sodium - ion batteries[J]. Small Methods, 2018, 3(4): 1800323.

[95] Cui R C, Xu B, Dong H J, et al. N/O dual-doped environment-friendly hard carbon as advanced anode for potassium-ion batteries[J]. Advanced Science, 2020, 7(5): 1902547.

[96] Tao L, Yang Y P, Wang H L, et al. Sulfur-nitrogen rich carbon as stable high capacity potassium ion battery anode: Performance and storage mechanisms[J]. Energy Storage Materials, 2020, 27: 212-225.

[97] Wang T D, Li Q, Feng Q T, et al. Carbon defects applied to potassium-ion batteries: A density functional theory investigation[J]. Nanoscale, 2021, 13(32): 13719-13734.

[98] Dong Y, Lin X J, Wang D K, et al. Modulating the defects of graphene blocks by ball-milling for ultrahigh gravimetric and volumetric performance and fast sodium storage[J]. Energy Storage Materials, 2020, 30: 287-295.

[99] Dong Y, Zhang S, Du X, et al. Boosting the electrical double - layer capacitance of graphene by self - doped defects through

ball - milling[J]. Advanced Functional Materials, 2019, 29(24): 1901127.

[100] Yuan R, Dong Y, Zhang S, et al. Efficient utilization of the active sites in defective graphene blocks through functionalization synergy for compact capacitive energy storage[J]. ACS Applied Materials & Interfaces, 2021, 13(48): 57092-57099.

[101] Yang Z, Ren X, Song Y, et al. Germanium - carbdiyne: A 3D well - defined sp - hybridized carbon - based material with superhigh Li storage property[J]. Energy & Environmental Materials, 2022(0): 1-8.

[102] Li G, Li Y, Liu H, et al. Architecture of graphdiyne nanoscale films[J]. Chemical Communications, 2010, 46(19): 3256-3258.

[103] Yi Y Y, Li J Q, Zhao W, et al. Temperature - mediated engineering of graphdiyne framework enabling high - performance potassium storage[J]. Advanced Functional Materials, 2020, 30(31): 2003039.

[104] Meng Y T, Nie C H, Guo W J, et al. Inorganic cathode materials for potassium ion batteries[J]. Materials Today Energy, 2022, 25: 100982.

[105] Liu S, Kang L, Jun S C. Challenges and strategies toward cathode materials for rechargeable potassium-ion batteries[J]. Advanced Materials, 2021, 33(47): 2004689.

[106] Qin L, Xiao N, Zheng J F, et al. Localized high - concentration electrolytes boost potassium storage in high - loading graphite[J]. Advanced Energy Materials, 2019, 9(44): 1902618.

[107] Ji B, Zhang F, Song X, et al. A novel potassium-ion-based dual-ion battery[J]. Advanced Materials, 2017, 29(19): 1700519.

[108] Fan L, Liu Q, Chen S, et al. Potassium-based dual ion battery with dual-graphite electrode[J]. Small, 2017, 13(30): 1701011.

[109] Beltrop K, Beuker S, Heckmann A, et al. Alternative electrochemical energy storage: Potassium-based dual-graphite batteries[J]. Energy & Environmental Science, 2017, 10(10): 2090-2094.

[110] Ding X, Zhang F, Ji B, et al. Potassium dual-ion hybrid batteries with ultrahigh rate performance and excellent cycling stability[J]. ACS Applied Materials & Interfaces, 2018, 10(49): 42294-42300.

[111] Liu X, Elia G A, Qin B S, et al. High-power Na-ion and K-ion hybrid capacitors exploiting cointercalation in graphite negative electrodes[J]. ACS Energy Letters, 2019, 4(11): 2675-2682.

[112] Fan L, Lin K, Wang J, et al. A nonaqueous potassium-based battery-supercapacitor hybrid device[J]. Advanced Materials, 2018, 30(20): 1800804.

[113] Zhang C, Liu X, Li Z, et al. Nitrogen - doped accordion - like soft carbon anodes with exposed hierarchical pores for advanced potassium - ion hybrid capacitors[J]. Advanced Functional Materials, 2021, 31(23): 2101470.

[114] Wang D K, Zhang J P, Li X T, et al. Woven microsphere architected by carbon nanotubes as high-performance potassium ion batteries anodes[J]. Chemical Engineering Journal, 2022, 429: 132272.